NASA TECHNICAL NOTE

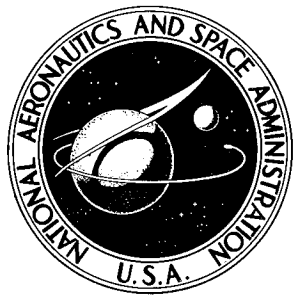

NASA TN D-6996

NASA TN D-6996

PREDICTION OF STATIC AERODYNAMIC CHARACTERISTICS FOR SPACE-SHUTTLE-LIKE AND OTHER BODIES AT ANGLES OF ATTACK FROM 0° TO 180°

by Leland H. Jorgensen

Ames Research Center
Moffett Field, Calif. 94035

NATIONAL AERONAUTICS AND SPACE ADMINISTRATION • WASHINGTON, D. C. • JANUARY 1973

1. Report No.	2. Government Accession No.	3. Recipient's Catalog No.
NASA TN D-6996		

4. Title and Subtitle	5. Report Date
PREDICTION OF STATIC AERODYNAMIC CHARACTERISTICS FOR SPACE-SHUTTLE-LIKE AND OTHER BODIES AT ANGLES OF ATTACK FROM 0° TO 180°	January 1973
	6. Performing Organization Code
7. Author(s)	8. Performing Organization Report No.
Leland H. Jorgensen	A-4500
	10. Work Unit No.
9. Performing Organization Name and Address	117-07-02-03-00-21
NASA Ames Research Center Moffett Field, Calif. 94035	11. Contract or Grant No.
	13. Type of Report and Period Covered
12. Sponsoring Agency Name and Address	Technical Note
National Aeronautics and Space Administration Washington, D. C. 20546	14. Sponsoring Agency Code

15. Supplementary Notes

16. Abstract

An engineering-type procedure is presented for computing normal-force, axial-force, and pitching-moment coefficients for bodies at angles of attack from 0° to 180°. The procedure is ideally suited for estimating the aerodynamic characteristics of space shuttle booster-like bodies because of the wide range of angles of attack, Mach numbers, and Reynolds numbers to be encountered. The analytical formulas, plots, and references given are also applicable for shuttle orbiter, missile, and aircraft-like bodies of both circular and noncircular cross section. The method for computing normal-force and pitching-moment coefficients is based upon the original proposal of Allen that the cross-flow or lift distribution over a body can be expressed as the sum of a slender-body potential term and an empirical viscous crossflow term.

Although experimental data from which to verify the procedure at very high angles of attack are extremely limited, the comparisons made thus far of computed with experimental results are good. In this report the procedure has been shown to be capable of predicting reasonably well the experimental variation of C_N, C_A, C_m, and x_{ac}/ℓ with angle of attack for nine bodies of revolution at a free-stream Mach number of 2.86.

17. Key Words (Suggested by Author(s))	18. Distribution Statement
Space shuttle Bodies High angles of attack Body theory	Unclassified – Unlimited

19. Security Classif. (of this report)	20. Security Classif. (of this page)	21. No. of Pages	22. Price*
Unclassified	Unclassified	44	$3.00

* For sale by the National Technical Information Service, Springfield, Virginia 22151

CONTENTS

SYMBOLS

A	cross-sectional (reference) area of cylindrical portion of body
A_b	body base area (at $x = \ell$)
A_p	planform area
A_s	surface wetted area
a, b	semimajor and semiminor axes of elliptic cross section, except in equation (28), where they are slopes of the semimajor and semiminor axes
C_A	axial-force coefficient, $\frac{F_a}{q_\infty A}$
C_a	axial-force coefficient, $\frac{F_a}{q_a A}$
C_{d_n}	crossflow drag coefficient of cylinder section, $\frac{F_n}{q_n(\Delta\ell_{cy})d_{cy}}$
C_m	pitching-moment coefficient about station at x_m from nose, $\frac{\text{pitching moment}}{q_\infty A\, d}$
C_N	normal-force coefficient, $\frac{F_n}{q_\infty A}$
C_p	pressure coefficient, $\frac{p-p_\infty}{q_\infty}$
d	body cross-section diameter
F_a, F_n	axial and normal forces
K	hypersonic similarity parameter, $\frac{M_\infty d}{\ell_N}$
k	corner rounding for body of square cross section, $\frac{r}{w}$
ℓ	body length

ℓ_N	nose length
ℓ_A	aftersection length
M_a	Mach number component in body axis direction, $M_\infty \cos \alpha$
M_n	Mach number component normal to body axis, $M_\infty \sin \alpha$
M_∞	free-stream Mach number
p	pressure
p_∞	free-stream static pressure
q_a	dynamic pressure component in body axis direction, $q_\infty \cos^2 \alpha$
q_n	dynamic pressure component normal to body axis, $q_\infty \sin^2 \alpha$
q_∞	free-stream dynamic pressure, $\frac{1}{2} \rho V_\infty^2$
r	nose or body cross-section radius for circular body or corner rounding for noncircular body
r_a	arc radius of ogive
r_b	nose or body cross-section radius at base
Re	free-stream Reynolds number based on body cross-section diameter, $\frac{\rho V_\infty d}{\mu}$
Re_a	Reynolds number component in body axis direction, $Re \cos \alpha$
Re_n	Reynolds number component normal to body axis, $Re \sin \alpha$
V	body volume
V_a	velocity component in body axis direction, $V_\infty \cos \alpha$
V_n	velocity component normal to body axis, $V_\infty \sin \alpha$
V_∞	free-stream velocity
w	body width
x	axial distance from body nose
x_{ac}	distance from nose to aerodynamic force center

x_c	distance from nose to centroid of body planform area
x_m	distance from nose to pitching-moment reference center
α	angle of attack
β	$\sqrt{M_\infty^2 - 1}$
γ	ratio of specific heats (taken as 1.4 for air)
η	crossflow drag proportionality factor
θ	cone half-angle
μ	dynamic viscosity of air
ρ	density of air
ϕ	angle of bank about body longitudinal axis

Subscripts

B	base
cir	circular cross section
cy	cylinder
Newt	Newtonian theory
SB	slender body theory
SF	skin friction
stag	stagnation
W	wave or pressure

PREDICTION OF STATIC AERODYNAMIC CHARACTERISTICS FOR SPACE-SHUTTLE-LIKE AND OTHER BODIES AT ANGLES OF ATTACK FROM 0° TO 180°

Leland H. Jorgensen

Ames Research Center

SUMMARY

An engineering-type procedure is presented for computing normal-force, axial-force, and pitching-moment coefficients for bodies at angles of attack from 0° to 180°. The procedure is ideally suited for estimating the aerodynamic characteristics of space shuttle booster-like bodies because of the wide range of angles of attack, Mach numbers, and Reynolds numbers to be encountered. The analytical formulas, plots, and references given are also applicable for shuttle orbiter, missile, and aircraft-like bodies of both circular and noncircular cross section. The method for computing normal-force and pitching-moment coefficients is based upon the original proposal of Allen that the crossflow or lift distribution over a body can be expressed as the sum of a slender-body potential term and an empirical viscous crossflow term.

Although experimental data from which to verify the procedure at very high angles of attack are extremely limited, the comparisons made thus far of computed with experimental results are good. In this report the procedure has been shown to be capable of predicting reasonably well the experimental variation of C_N, C_A, C_m, and x_{ac}/ℓ with angle of attack for nine bodies of revolution at a free-stream Mach number of 2.86.

The procedure can be used to predict the effects of Mach number and Reynolds number changes on the aerodynamic coefficients of shuttle boosters from atmospheric entry to recovery. For a booster-like body of revolution (fineness ratio 5 ogival nose with a fineness ratio 6 cylinder afterbody) effects of Mach number and Reynolds number on the variation of C_N and x_{ac}/ℓ with α have been computed and are presented for illustration.

It is predicted that Mach number changes from $M_\infty = 7$ down to $M_\infty = 0.3$ (the entry range studied) can significantly affect C_N over most of the α range. The aerodynamic force center, however, moves little with the Mach number.

Even more pronounced than the effect of Mach number is the effect of Reynolds number, which has been predicted for the body at the subcritical Mach number of $M_\infty \simeq 0.3$. With increase in Reynolds number from 10^5 to 10^6, up to about 75 percent of the normal force is lost, the maximum loss occurring at $\alpha = 90°$. With further increase in Reynolds number to $Re = 10^7$, only about one-half of the normal force at $Re = 10^5$ is regained. This large effect of Reynolds number results from the fact that the crossflow Reynolds numbers vary from subcritical to critical as free-stream Reynolds number increases well over $Re = 10^5$.

The fact that there can be a severe effect of Reynolds number on the aerodynamics when the crossflow Reynolds numbers are in the critical range also has been demonstrated with experimental results for a flat-bottomed, shuttle-type body. Computed normal-force coefficients for this body at $M_\infty = 0.3$ qualitatively predict the significant measured effect of changing the crossflow Reynolds number through the critical range.

The results of this investigation suggest that, if shuttle boosters (and other vehicles) are to be flown back into the atmosphere at very high angles of attack to low subsonic Mach numbers, effort should be made to obtain wind-tunnel data at near-flight Reynolds numbers.

INTRODUCTION

In some recent studies of space-shuttle booster reentry profiles, the booster angle of attack varies from about 70° or 80° down to 0°, and the Mach number ranges from about 7 or 8 down to a low subsonic recovery or flyback value. The Reynolds numbers based on body diameter are greater than 1 million over most of the reentry profile. Prediction of the aerodynamic forces and moments through such a wide range of conditions presents an engrossing challenge.

For booster-like bodies at the higher angles of attack, it has been shown from wind-tunnel tests (e.g., refs. 1-3) that the aerodynamic force and moment characteristics can be affected considerably by changes in Mach and Reynolds numbers. At hypersonic Mach numbers it appears that the characteristics can be predicted acceptably well by programs utilizing Newtonian theory (e.g., ref. 2). The real need now appears to be in the formulation and validation of analytical prediction techniques applicable to lower Mach numbers. Of concern also is the prediction of Reynolds number effects on the aerodynamics, particularly at subsonic Mach numbers where the Reynolds numbers based on diameter can become very large (of the order of 10^7 to 10^8). Recent experimental tests have shown that Reynolds number can significantly alter the aerodynamic characteristics of a shuttle-like, flat-bottomed body both with and without wing and tail at subsonic Mach numbers below about 0.6 (ref. 3).

In view of the foregoing, the present study was initiated to accomplish the following objectives:

(1) Present an engineering-type procedure for computing the normal force, axial force, and pitching-moment coefficients of booster-like bodies of circular and noncircular cross section at Mach numbers, Reynolds numbers, and angles of attack expected during reentry.

(2) Compare computed results by this procedure with available experimental data (ref. 4) for nine bodies of revolution tested in a wind tunnel at a Mach number of 2.86, a Reynolds number of 1.25×10^5, and angles of attack from 0° to 180°.

(3) Point out how changes in Mach and Reynolds numbers can be expected to alter the aerodynamic coefficients of booster bodies.

PROCEDURE AND FORMULAS FOR COMPUTING AERODYNAMIC CHARACTERISTICS

Prior to the work of Allen in 1949-51 (refs. 5 and 6), most analytical procedures for computing the aerodynamic characteristics of bodies and missile-type configurations were based on potential theory and were limited in usefulness to very low angles of attack. Allen proposed a method for predicting the forces and moments for bodies of revolution inclined to angles of attack considerably higher than those for which theories based only on potential-flow concepts are known to apply. In this method a crossflow lift attributed to flow separation is added to the lift predicted by slender-body potential theory. This method has been used quite successfully in estimating the aerodynamic coefficients of inclined bodies (e.g., refs. 5-9), although most data available for study have been for bodies at angles of attack below about 20°. In the present investigation, Allen's method has been adopted and formulas have been written for computing the normal-force, axial-force, and pitching-moment coefficients for bodies throughout the angle of attack range from 0° to 180°.

General Expressions for Bodies of Revolution at Angles of Attack from 0° to 180°

For the sign convention in sketch (a), normal-force, axial-force, and pitching-moment coefficients are given by

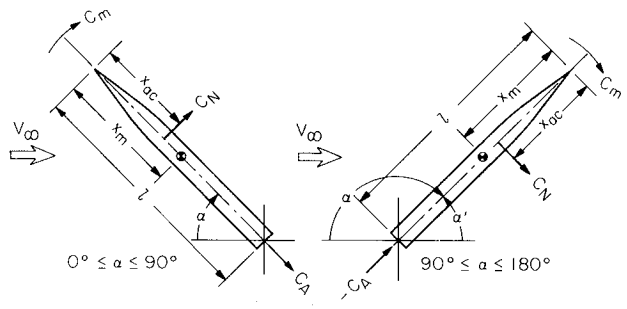

Sketch (a)

$$C_N = \frac{A_b}{A} \sin 2\alpha' \cos\frac{\alpha'}{2} + \eta C_{d_n} \frac{A_p}{A} \sin^2 \alpha'; \quad 0° \leqslant \alpha \leqslant 180° \tag{1}$$

$$C_A = C_{A_{\alpha=0°}} \cos^2 \alpha'; \qquad 0° \leqslant \alpha \leqslant 90° \tag{2}$$

$$C_A = C_{A_{\alpha=180°}} \cos^2 \alpha'; \qquad 90° \leqslant \alpha \leqslant 180° \tag{3}$$

$$C_m = \left[\frac{V-A_b(\ell-x_m)}{A\,d}\right] \sin 2\alpha' \cos\frac{\alpha'}{2} + \eta\, C_{d_n} \frac{A_p}{A}\left(\frac{x_m-x_c}{d}\right)\sin^2\alpha'; \qquad 0^\circ \leqslant \alpha \leqslant 90^\circ \qquad (4)$$

and

$$C_m = -\left(\frac{V-A_b x_m}{A\,d}\right) \sin 2\alpha' \cos\frac{\alpha'}{2} + \eta\, C_{d_n} \frac{A_p}{A}\left(\frac{x_m-x_c}{d}\right)\sin^2\alpha'; \quad 90^\circ \leqslant \alpha \leqslant 180^\circ \qquad (5)$$

where

$$\alpha' = \alpha \text{ for } 0^\circ \leqslant \alpha \leqslant 90^\circ \text{ and } \alpha' = 180^\circ - \alpha \text{ for } 90^\circ \leqslant \alpha \leqslant 180^\circ$$

The aerodynamic force center is given by

$$x_{ac} = \left(\frac{x_m}{d} - \frac{C_m}{C_N}\right) d \qquad (6)$$

The first terms in equations (1), (4), and (5) come from slender-body potential theory. The second terms represent the viscous crossflow or crossflow attributed to flow separation.

Crossflow drag coefficient – In the expressions for C_N and C_m (eqs. (1), (4), and (5)) C_{d_n} is the crossflow drag coefficient for a section of an "infinite" length cylinder placed normal to an airstream. It is a function of both the Mach number and Reynolds number components that are normal to the cylinder longitudinal axis, and, hence, for a body at angle of attack it is a function of

$$M_n = M_\infty \sin\alpha \qquad (7)$$

and

$$Re_n = Re \sin\alpha \qquad (8)$$

M_n is commonly called the crossflow Mach number and Re_n the crossflow Reynolds number.

For circular cylinders, "state-of-the knowledge" plots have been prepared for the variation of C_{d_n} with M_n and Re_n (figs. 1-3). Figure 1 gives the variation of C_{d_n} with M_n over the entire reentry Mach number range expected for a booster body (i.e., maximum M_n from about 7 or 8 down to almost 0). It was prepared from the data of references 10 through 15. Also shown for reference are the theoretical variations predicted from Newtonian and modified Newtonian theories. Because of

the close agreement of the Newtonian values with experiment at the higher Mach numbers, it is not surprising that programs utilizing Newtonian theory have been used to successfully predict shuttle-booster wind-tunnel results at hypersonic Mach numbers (see, e.g., ref. 2). Except for the transonic range, where reliable data are very limited, the variation of C_{d_n} with M_n is well documented in figure 1. There is, however, a crossflow Reynolds number effect which can drastically lower the values of C_{d_n} at M_n below about 0.5. For M_n less than about 0.5 and Re_n greater than about 10^5, the values of C_{d_n} are given in greater detail in figures 2 and 3.

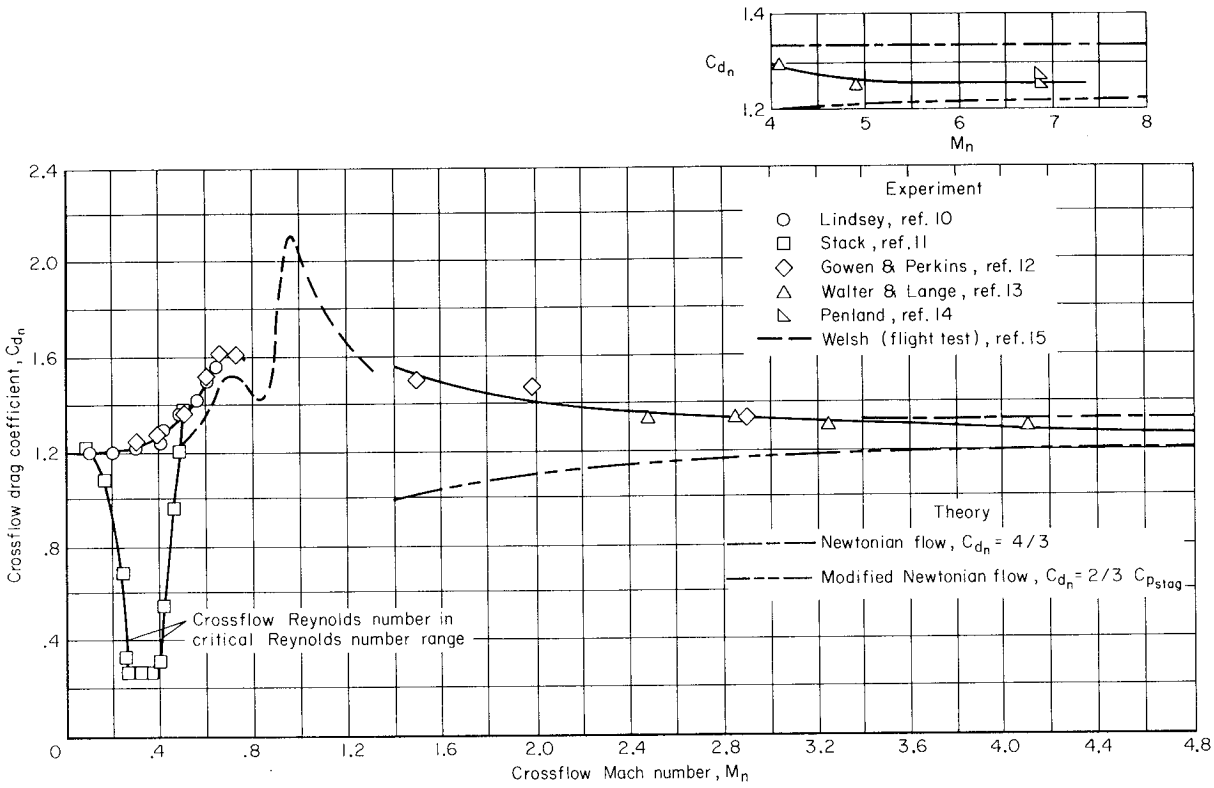

Figure 1. – Variation of crossflow drag coefficient with crossflow Mach number for circular cylinders.

Figure 2 gives the variation of C_{d_n} with Re_n for M_n less than about 0.4. It has been well documented over the last 58 years (e.g., refs. 11, 16-18) that $C_{d_n} \simeq 1.2$ for laminar boundary-layer flow and separation just before the critical Reynolds number of about $Re_n = 2\times10^5$. At about $Re = 5\times10^5$ there is evidence (e.g., refs. 19-21) of laminar boundary-layer flow around the front of the cylinder to an angular position of about 80° or 90° where the flow separates, undergoes transition, and reattaches at an angular position of about 110° to form a laminar separation bubble. Then the turbulent flow separates at some position downstream (an angular location of about 130°). With further increase in Reynolds number into the supercritical regime, the bubble decreases in size until the transition to turbulent flow moves upstream of the location of laminar separation, and the bubble disappears (ref. 21). From the low C_{d_n} value between about 0.15 and 0.30, C_{d_n} increases gradually, at least for increase in Re_n up to about 5×10^6. The supercritical Reynolds number regime has only been investigated recently in any detail (refs. 18-21), and there is still considerable uncertainty in the

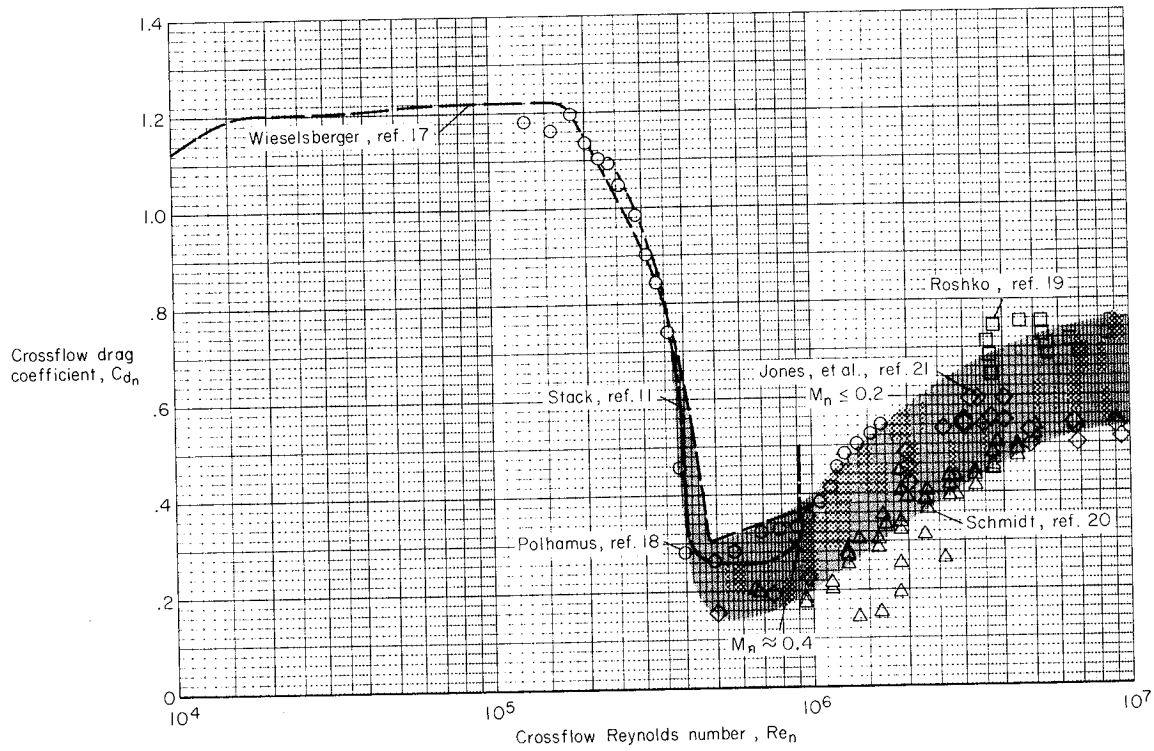

Figure 2. – Variation of crossflow drag coefficient with crossflow Reynolds number for circular cylinders at subcritical crossflow Mach numbers ($M_n \leq 0.4$).

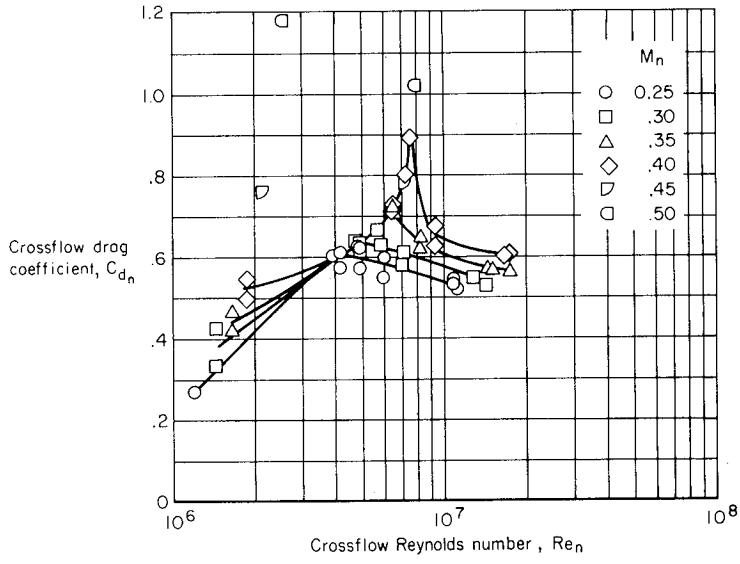

Figure 3. – Variation of crossflow drag coefficient with crossflow Reynolds number for circular cylinders at supercritical Reynolds numbers and at crossflow Mach numbers from 0.25 to 0.50 (from Jones, Cincotta, and Walker, ref. 21).

magnitude and trend of C_{d_n} with Re_n and M_n. The shading in figure 2 indicates the approximate spread or uncertainty in C_{d_n} based on known data.

Jones, Cincotta, and Walker (ref. 21) have probably made the most detailed study of circular cylinders in supercritical flow. With the use of freon gas for obtaining high Re_n, they have shown that there is an effect of M_n on the variation of C_{d_n} with Re_n. Figure 3 (taken from ref. 21) summarizes their C_{d_n} results for M_n from 0.25 to 0.50. The reader is referred to reference 21 for their interpretation of these C_{d_n} results based upon pressure-distribution and visual-flow studies.

Crossflow drag proportionality factor – In equations (1), (4), and (5) η is the crossflow drag proportionality factor, that is, the ratio of the crossflow drag coefficient for a finite length cylinder to that for an infinite length cylinder. Cylinder drag coefficients from which values of η can be determined have been measured, to the author's knowledge, only at very low subsonic Mach numbers (refs. 22 and 23). In figure 4, values of η from reference 22 are plotted as a function of length-to-diameter ratio. For reference, η's for flat plates are also presented (plotted as a function of plate length-to-width ratio). In spite of a dearth of η data throughout the subsonic Mach number regime, the results given in figure 4 have been used to successfully predict, for most engineering purposes, the aerodynamic characteristics of bodies of revolution at subsonic Mach numbers (e.g., ref. 24). For bodies at supersonic and hypersonic Mach numbers, η probably can be assumed to be unity, an assumption indicated as being essentially correct from past investigations (e.g., refs. 5, 7, 9, and 24).

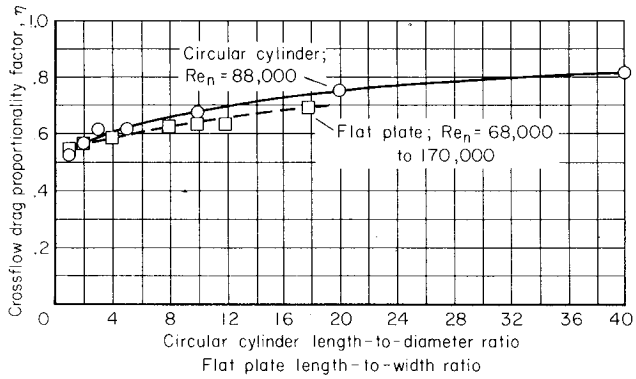

Figure 4. – Ratio of crossflow drag coefficient for a finite length cylinder (or flat plate) to that for an infinite length cylinder (or flat plate), from ref. 22.

Relative influence of crossflow terms – From a strict theoretical standpoint, an argument can be made against the addition of a theoretically derived potential crossflow term to an empirically determined viscous crossflow term (eqs. (1), (4), and (5)), especially at very high angles of attack. The argument is that the empirical term actually encompasses all of the crossflow (viscous and nonviscous), since it is determined from experimental measurements of total crossflow drag. The Allen approach, however, has been justified on the basis of rather good agreement with existing experimental lift and pitching-moment data for bodies at angles of attack up to about $\alpha = 20°$. At higher α, however, the approach has had little or no verification, but logic dictates that it should give increasingly better results as α increases to 90°. The viscous crossflow (empirical) term contributes most of the normal force as α increases and, in fact, all of the normal force at $\alpha = 90°$.

For demonstration, the relative influence of the crossflow terms in the C_N and C_m expressions (equations (1), (4), and (5)) has been calculated for an ogive-cylinder body of fineness ratio 11 ($\ell_N/d = 5$) at angles of attack from 0° to 180° and $M_\infty = 2.9$. Computed magnitudes from the slender-body potential and viscous crossflow terms are presented in figure 5. It is seen that the slender-body

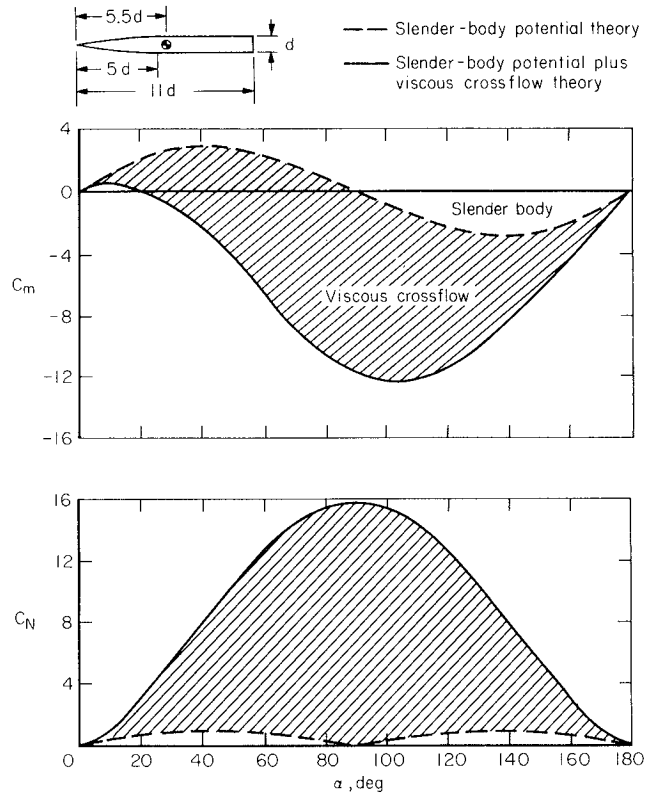

Figure 5. – Theoretical components of normal force and pitching-moment coefficients for an ogive-cylinder body at angles of attack from 0° to 180° and $M_\infty = 2.9$.

term contributes relatively little to C_N at high α, but it has a significant influence on C_m. Because of the strong influence of both the potential and viscous crossflow terms on the variation of C_m with α, experimental verification of equations (4) and (5) for determining C_m is especially pertinent.

Axial-Force Coefficients for Bodies of Revolution at Angles of Attack of 0° and 180°

To predict the variation of C_A with angle of attack by equations (2) and (3), either computed or measured values of axial-force coefficient at α of 0° and 180° are required. In general the axial-force coefficient at $\alpha = 0°$ or 180° can be expressed by

$$C_A = C_{A_W} + C_{A_{SF}} + C_{A_B} \tag{9}$$

where C_{A_W} represents the wave or pressure contribution from the nose or forwardfacing base; $C_{A_{SF}}$ is the skin-friction contribution; and C_{A_B} is the base-pressure contribution.

For the present study, cylindrical bodies of revolution with conical, ogival, and flat-faced noses have been emphasized, and so in this section of the report consideration is given to these types of bodies. In spite of the extensive literature on the subject of body drag, only a few pertinent sources of information are cited herein, and the desire is to cite simple formulas and correlations from which practical engineering-type answers can be readily obtained. Because of lack of simple formulas, correlations, and indeed reliable theory for transonic Mach numbers, axial-force coefficients for this regime are not considered in the present report.

Wave or pressure contribution – For a forwardfacing conical-nosed body at supersonic or hypersonic Mach numbers, the wave or pressure contribution to the total axial-force coefficient can be readily computed from the Linnell-Bailey expression (ref. 25)

$$C_{A_W} = \frac{(4 \sin^2 \theta)(2.5 + 8\beta \sin \theta)}{(1 + 16\beta \sin \theta)} \tag{10}$$

where $\beta = \sqrt{M_\infty^2 - 1}$ and θ is the cone half-angle. This equation was obtained from correlation of computed values of C_p $(=C_{A_W})$ from exact (Taylor-Maccoll) cone theory. According to Wittcliff (ref. 26) it provides a root-mean-square accuracy of 1.4 percent over the range of $0.05 \leqslant \beta \sin \theta \leqslant 10$. Wittcliff (ref. 26) and Schwartz (ref. 27) also present equally or more accurate correlation expressions.

For a circular-arc tangent ogive nose at high supersonic and hypersonic M_∞, values of C_{A_W} can be determined from the correlation curve in figure 6. Here the wave drag parameter, $(\gamma/2) M_\infty^2 \, C_{A_W}$,

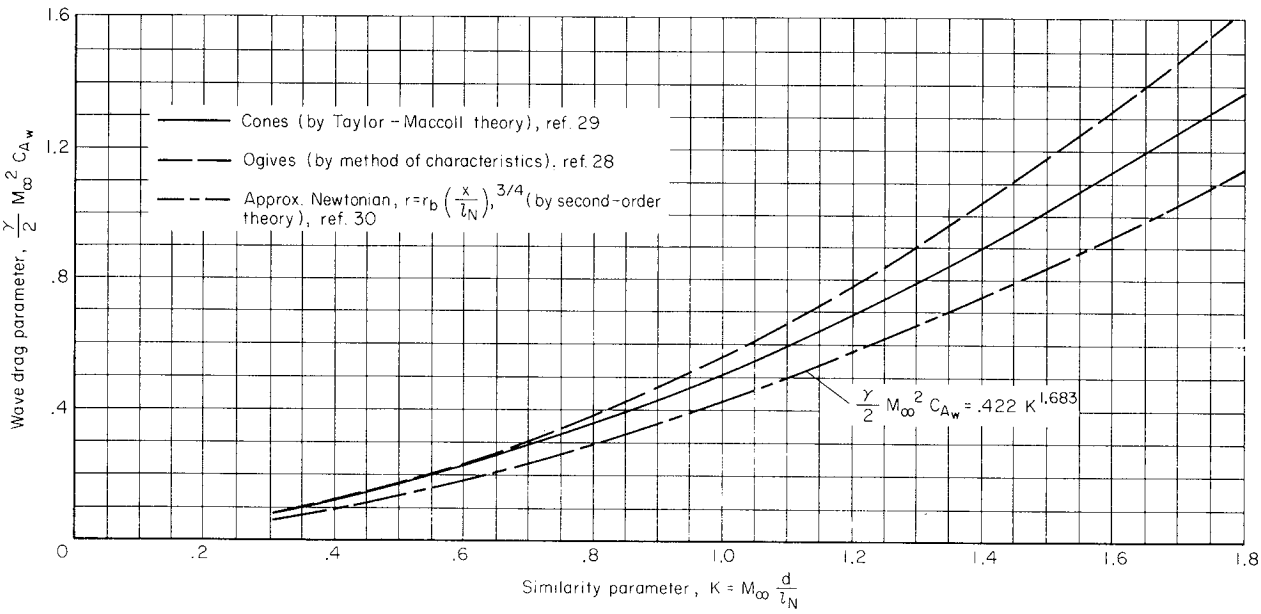

Figure 6. – Variation of wave drag parameter with hypersonic similarity parameter for cones, circular-arc tangent ogives, and approximate minimum-drag Newtonian noses at $\alpha = 0°$.

is plotted as a function of the hypersonic similarity parameter, $K = M_\infty(d/\ell_N)$. This correlation curve was obtained by Rossow (ref. 28) from values of C_{AW} computed by the method of characteristics. Also shown for reference in figure 6 are correlation curves for cones (ref. 29) and Newtonian minimum-drag noses optimized for specified length and base diameter (ref. 30)

For a body with a flat-faced nose or flat base forward, it can be assumed that the stagnation pressure coefficient $C_{p_{stag}}$ is nearly constant over the flat face, so that $C_{AW} \simeq C_{p_{stag}}$. With the aid of references 31 and 32, the variation of $C_{p_{stag}}$ with free-stream Mach number has been computed for perfect air, and the results are plotted in figure 7. For equilibrium real air, there are many tables and charts from which one can compute the variation of $C_{p_{stag}}$ with free-stream velocity and altitude (e.g., ref. 33). However, for preliminary studies and for most of the booster range of flow conditions, the perfect air plot in figure 7 is probably satisfactory.

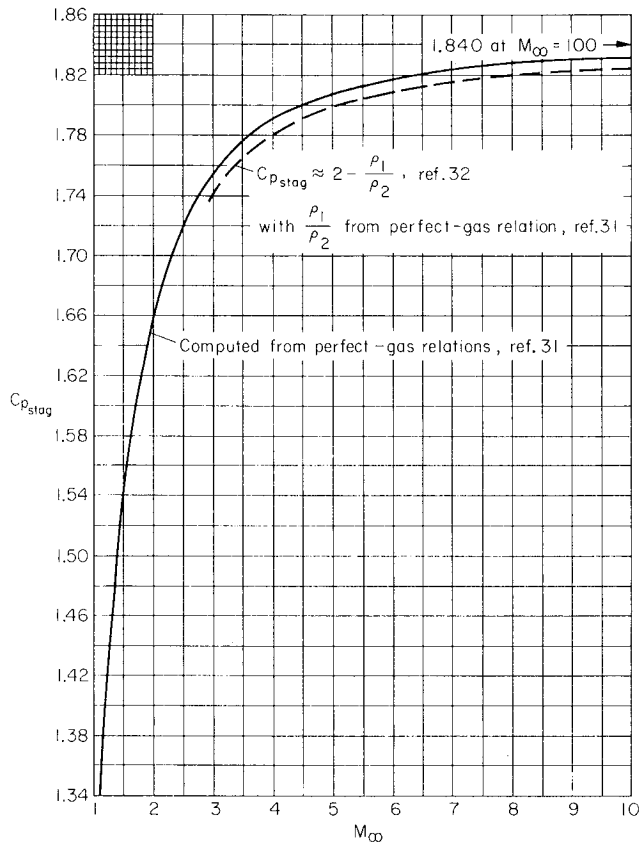

Figure 7. – Variation of stagnation pressure coefficient with free-stream Mach number

Readers who are interested in obtaining computed drag coefficients for other nose shapes and bodies of revolution, including some with boattailing, might refer to Stivers' work (ref. 34). Stivers has used the method of characteristics to compute pressure coefficients and drag coefficients for 18 constant length and volume slender bodies of revolution for Mach numbers from 2 to 12.

Skin-friction contribution – The skin-friction contribution, $C_{A_{SF}}$, can be readily computed by any number of classical flat-plate methods outlined in, for example, references 35 through 41. For most boosters it is probably realistic to assume a turbulent boundary layer and compute the skin friction by either the T' method (refs. 35 and 36), the Spalding and Chi method (refs. 38 and 39), or the second method of Van Driest (refs. 37, 40, and 41). From comparison of these methods with direct measurements of skin friction, Hopkins and Inouye (ref. 40) suggest that the Van Driest method (II) be used to predict the turbulent skin friction for the design of supersonic and hypersonic vehicles. Hopkins (ref. 41) has prepared charts by the Van Driest method (II) from which skin-friction coefficients can be readily obtained.

Base pressure contribution – For blunt-based bodies in supersonic flow, Gabeaud (ref. 42) derived the following expression for base pressure coefficient:

$$C_{p_B} = \frac{2}{\gamma M_\infty^2}\left\{\left(\frac{2}{\gamma+1}\right)^{1.4}\left(\frac{1}{M_\infty}\right)^{2.8}\left[\frac{2\gamma M_\infty^2-(\gamma-1)}{\gamma+1}\right]-1\right\} \tag{11}$$

This expression, which predicts a perfect vacuum at $M_\infty = \infty$, has been verified reasonably well by experimental data. In figure 8 it is seen to agree closely with results compiled by Love (ref. 43) for nonboattailed bodies of revolution with turbulent boundary layers for Mach numbers down to about $M_\infty = 1.5$. With $C_{A_B} = -C_{p_B}$, either equation (11) or the results in figure 8 can be used to predict C_{A_B}.

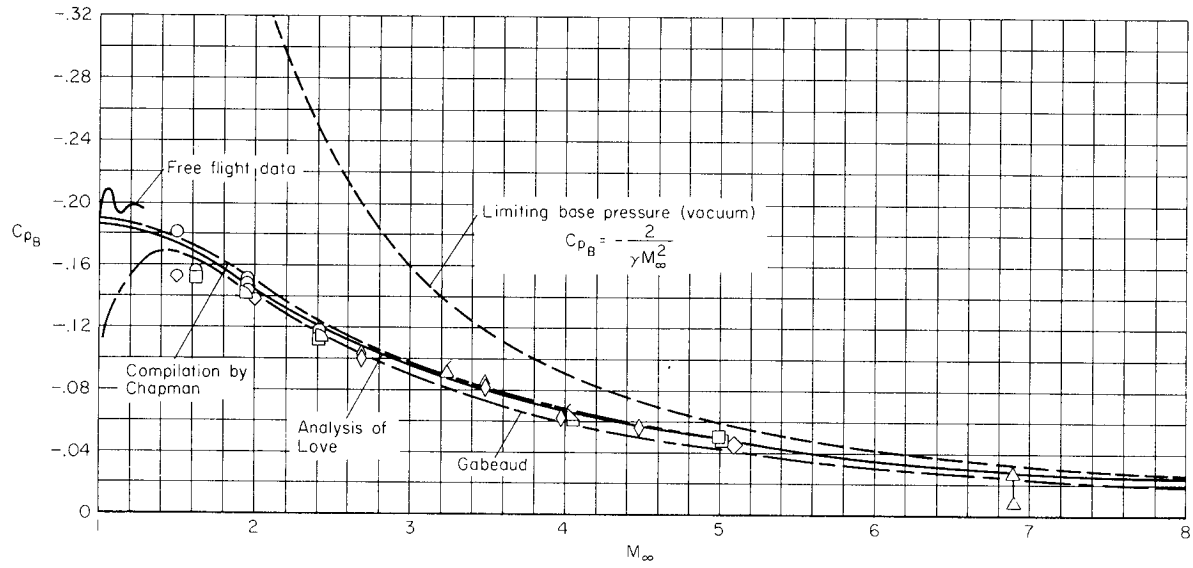

Figure 8. – Variation of base pressure coefficient with free-stream Mach number for bodies of revolution having cylindrical afterbodies at $\alpha = 0°$ (from Love, ref. 43, except for curve computed from Gabeaud, ref. 42).

For boattailed bodies of revolution in supersonic flow, Love (ref. 43) has devised a simple procedure for determining base-pressure coefficients. His method, originally applied only to supersonic flow, has recently been extended by Stivers (ref. 34) to hypersonic flow.

Alternate Procedure for Computing Axial-Force Coefficients for Bodies of Revolution at Angles of Attack

An alternate, more precise, procedure than the use of equations (2) and (3) can be used to compute the variation of C_A with α. In this procedure the axial-force coefficient is determined from the components of Mach number and Reynolds number in the body axial direction and is expressed by

$$C_A = C_a \cos^2 \alpha \tag{12}$$

where

$$C_a = \frac{F_a}{q_a A} = C_{a_W} + C_{a_{SF}} + C_{a_B} \tag{13}$$

with

$$C_{a_W} = f(M_a, \ell_N/d) \tag{14}$$

$$C_{a_{SF}} = f(M_a, Re_a, A_s/A) \tag{15}$$

$$C_{a_B} = f(M_a) \text{ for turbulent boundary layer} \tag{16}$$

$$q_a = \frac{1}{2} \rho V_a^2 = q_\infty \cos^2 \alpha \tag{17}$$

$$M_a = M_\infty \cos \alpha \tag{18}$$

and

$$Re_a = Re \frac{\ell}{d} \cos \alpha \tag{19}$$

Here C_{a_W} is the wave or force-pressure contribution to the axial-force coefficient; $C_{a_{SF}}$ is the skin-friction contribution from the body wetted area; and C_{a_B} is the base-pressure contribution. These axial-force components are based on the axial component q_a of the dynamic pressure and are determined from axial components (M_a and Re_a) of free-stream Mach number (M_∞) and Reynolds number (Re).

Estimation of Aerodynamic Characteristics for Bodies with Noncircular Cross Sections

Equations (1) through (5) can be adapted for the determination of the aerodynamic characteristics of slender bodies of noncircular cross section if values of C_{d_n} are available for the cross sections considered. At low subsonic crossflow Mach numbers, the variation of C_{d_n} with Re_n has been measured for many cross sections of interest (see, e.g., refs. 10, 18, 44, 45, and 46). However, there are little or no data available for the variation of C_{d_n} with M_n over the moderate subsonic to hypersonic range. In view of this lack of data, an alternate procedure has been suggested by Jorgensen (ref. 9) for computing C_N and C_m.

C_N and C_m controlled by crossflow Mach number – In the procedure of reference 9, the force and moment coefficients are computed for the equivalent body of circular cross section that has the same axial distribution of cross-sectional area as the noncircular body. Then the values of C_N and C_m for the noncircular body are computed with the use of values of $C_N/(C_N)_{cir}$ $(=C_m/(C_m)_{cir})$ determined from apparent mass coefficients (slender-body theory). Very good agreement of theory with experiment has been obtained by this procedure for bodies of elliptic cross section at the conditions investigated in reference 9 (a/b from 1 to 2, ϕ of 0° and 90°, M_∞ from 2 to 4, and α from 0° to 20°). In the next few paragraphs, several formulas are given from which values of $C_N/(C_N)_{cir}$ can be computed for bodies of elliptic and square cross section.

From slender-body theory, the ratio of C_N for a body of elliptic cross section to C_N for the equivalent body of circular cross section is given by

$$\frac{C_N}{(C_N)_{cir}} = \frac{C_m}{(C_m)_{cir}} = \frac{a}{b}\cos^2\phi + \frac{b}{a}\sin^2\phi \tag{20}$$

where ϕ is the angle of bank about the body longitudinal axis, being 0° with the semimajor axis a perpendicular to the crossflow velocity, and 90° with the semiminor axis perpendicular to the crossflow velocity. (See sketches (b) and (c).)

For bodies at very high α in hypersonic flow, it is likely that values of $C_N/(C_N)_{cir}$ $(=C_m/(C_m)_{cir})$ will be given more accurately from Newtonian theory than from slender-body theory. In the present study the following two equations for elliptic cross sections have been derived from Newtonian theory.

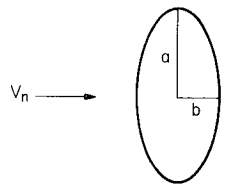

Sketch (b)

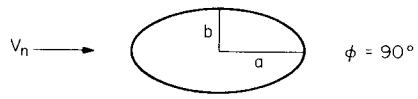

Sketch (c)

With the semimajor axis a perpendicular to the crossflow velocity,

$$\frac{C_N}{(C_N)_{cir}} = \frac{C_m}{(C_m)_{cir}} = \frac{3}{2}\sqrt{\frac{a}{b}}\left\{\frac{-b^2/a^2}{\left(1-\frac{b^2}{a^2}\right)^{3/2}}\log\left[\frac{a}{b}\left(1+\sqrt{1-\frac{b^2}{a^2}}\right)\right]+\frac{1}{1-\frac{b^2}{a^2}}\right\} \tag{21}$$

With the semiminor axis b perpendicular to the crossflow velocity,

$$\frac{C_N}{(C_N)_{cir}} = \frac{C_m}{(C_m)_{cir}} = \frac{3}{2}\sqrt{\frac{b}{a}}\left[\frac{a^2/b^2}{\left(\frac{a^2}{b^2}-1\right)^{3/2}}\tan^{-1}\left(\sqrt{\frac{a^2}{b^2}-1}\right)-\frac{1}{\frac{a^2}{b^2}-1}\right] \tag{22}$$

Values of $C_N/(C_N)_{cir}$ computed from slender-body and Newtonian theories for various a/b are compared in tables 1 and 2.

TABLE 1. – $C_N/(C_N)_{cir}$ FOR ELLIPTIC CROSS SECTION WITH SEMIMAJOR AXIS a PERPENDICULAR TO CROSSFLOW VELOCITY

$\frac{a}{b}$	$C_N/(C_N)_{cir}$		Percent difference $\left(\frac{\text{Slender-body}-\text{Newtonian}}{\text{Slender-body}}\right)100$
	Slender-body theory	Newtonian theory	
$\sqrt{2}$	1.41	1.34	5
1.5	1.50	1.41	6
2	2.00	1.75	12
3	3.00	2.32	23

TABLE 1. – $C_N/(C_N)_{cir}$ FOR ELLIPTIC CROSS SECTION WITH SEMIMAJOR

AXIS a PERPENDICULAR TO CROSSFLOW VELOCITY – Concluded

$\frac{a}{b}$	$C_N/(C_N)_{cir}$		Percent difference $\left(\frac{\text{Slender-body–Newtonian}}{\text{Slender-body}}\right)100$
	Slender-body theory	Newtonian theory	
4	4.00	2.77	31
5	5.00	3.17	37
6	6.00	3.52	41

TABLE 2. – $C_N/(C_N)_{cir}$ FOR ELLIPTIC CROSS SECTION WITH SEMIMINOR

AXIS b PERPENDICULAR TO CROSSFLOW VELOCITY

$\frac{a}{b}$	$C_N/(C_N)_{cir}$		Percent difference $\left(\frac{\text{Slender-body–Newtonian}}{\text{Slender-body}}\right)100$
	Slender-body theory	Newtonian theory	
$\sqrt{2}$	0.707	0.720	−2
1.5	.667	.679	−2
2	.500	.501	0
3	.333	.316	5
4	.250	.222	11
5	.200	.167	16
6	.167	.132	21

For bodies with square cross sections in which the corners are rounded (see sketch (d)), Newtonian theory gives

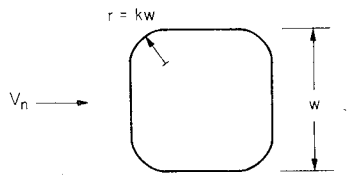

Sketch (d)

$$\frac{C_N}{(C_N)_{cir}} = \frac{C_m}{(C_m)_{cir}} = \frac{1}{2}\left(\frac{3}{2} - k\right)\sqrt{\frac{\pi}{1-(4-\pi)\,k^2}} \quad ;$$

$$0 \leqslant k \leqslant 0.5 \qquad (23)$$

where the diameter of the equivalent circular body is

$$d = 2w\sqrt{\frac{1-(4-\pi)k^2}{\pi}} \tag{24}$$

Some values of $C_N/(C_N)_{cir}$ from equation (23) are given in table 3.

TABLE 3. – $C_N/(C_N)_{cir}$ FROM NEWTONIAN THEORY FOR SQUARE CROSS SECTIONS WITH ROUNDED CORNERS

k	0	0.05	0.1	0.2	0.3	0.4	0.5
$C_N/(C_N)_{cir}$	1.33	1.29	1.25	1.17	1.11	1.05	1.00

Corresponding values from slender-body theory vary from 1.19 at $k = 0$ (no corner radius) to 1.00 at $k = 0.5$ (completely circular cross section).

For noncircular bodies, an approach somewhat consistent with the logic of each term in equations (1), (4), and (5) is to modify the first term by $C_N/(C_N)_{cir}$ $(= C_m/(C_m)_{cir})$ from slender-body theory and the second term by $C_N/(C_N)_{cir}$ $(=C_m/(C_m)_{cir})$ from Newtonian theory. The equations then become,

$$C_N = \left(\frac{A_b}{A}\sin 2\alpha' \cos\frac{\alpha'}{2}\right)\left[\frac{C_N}{(C_N)_{cir}}\right]_{SB} + \left(\eta C_{d_n}\frac{A_b}{A}\sin^2\alpha'\right)\left[\frac{C_N}{(C_N)_{cir}}\right]_{Newt}; \quad 0^\circ \leqslant \alpha \leqslant 180^\circ \tag{25}$$

$$C_m = \left\{\left[\frac{V - A_b(\ell - x_m)}{Ad}\right]\sin 2\alpha' \cos\frac{\alpha'}{2}\right\}\left[\frac{C_m}{(C_m)_{cir}}\right]_{SB} + \left[\eta C_{d_n}\frac{A_p}{A}\left(\frac{x_m - x_c}{d}\right)\sin^2\alpha'\right]\left[\frac{C_m}{(C_m)_{cir}}\right]_{Newt}; \quad 0^\circ \leqslant \alpha \leqslant 90^\circ \tag{26}$$

and

$$C_m = -\left[\left(\frac{V - A_b x_m}{Ad}\right) \sin 2\alpha' \cos\frac{\alpha'}{2}\right]\left[\frac{C_m}{(C_m)_{cir}}\right]_{SB} + \left[\eta C_{d_n} \frac{A_p}{A}\left(\frac{x_m - x_c}{d}\right) \sin^2 \alpha'\right]\left[\frac{C_m}{(C_m)_{cir}}\right]_{Newt}; \quad 90° \leqslant \alpha \leqslant 180° \qquad (27)$$

where $\alpha' = \alpha$ for $0° \leqslant \alpha \leqslant 90°$ and $\alpha' = 180° - \alpha$ for $90° \leqslant \alpha \leqslant 180°$.

For many cross sections the values of $C_N/(C_N)_{cir}$ $(=C_m/(C_m)_{cir})$ given from slender-body theory are reasonably close to those given from Newtonian theory, (see, e.g., tables 1-3), and the distinction between these theories in equations (25) through (27) may not be necessary for many engineering-type studies.

It should be noted that equations (25) through (27) are written for the case of a body whose cross-sectional shape is the same along its length. The cross-sectional area, of course, need not be constant over the body length.

C_N and C_m controlled by crossflow Reynolds number – At low subsonic crossflow Mach numbers (below critical) the variation of C_{d_n} with Re_n for the cross section of interest can be significantly large as Re_n exceeds the critical value. (See, for example, fig. 2 for a circular cross section.) For the Reynolds number controlled conditions, equations (25) through (27) can be used with slight modification to the second terms. The values of $\left[C_N/C_N)_{cir}\right]_{Newt}$ and $\left[C_m/(C_m)_{cir}\right]_{Newt}$ become unity, and experimental values of C_{d_n} for the cross section of interest are used. It should be noted, however, that most experimental values of C_{d_n} are based on cross section width w and must be multiplied by w/d, where d is the equivalent diameter of the cross section.

In table 4 some references are listed from which experimental values of C_{d_n} versus Re_n can be obtained for various cross sections and flow directions.

Crossflow drag proportionality factor – Based upon experience with bodies of elliptic, square, and triangular cross section at supersonic freestream Mach numbers (ref. 9), it is probably best to assume a crossflow drag proportionality factor η of unity for bodies in supersonic and hypersonic freestream flow. For subsonic freestream flow, η can be interpolated from figure 4, since the values plotted as a function of length-to-width ratio (fig. 4) are only slightly lower for flat plates than for circular cylinders. However, the reliability of using figure 4 for obtaining η for noncircular bodies has not been verified, and it is likely that η varies somewhat with crossflow Mach number and/or crossflow Reynolds number as well as with length-to-width ratio.

TABLE 4. – REFERENCES FROM WHICH EXPERIMENTAL VALUES OF C_{d_n} VS Re_n CAN BE OBTAINED FOR VARIOUS CROSS SECTIONS AND FLOW DIRECTIONS

References	Cross sections and flow directions
10 (Lindsey)	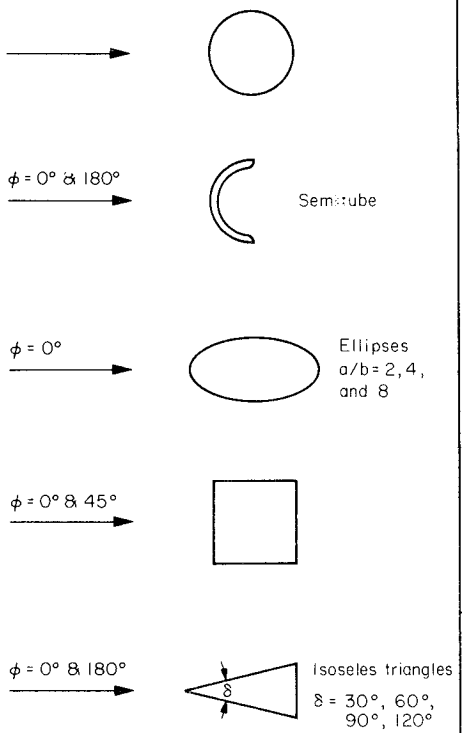
18 (Polhamus)	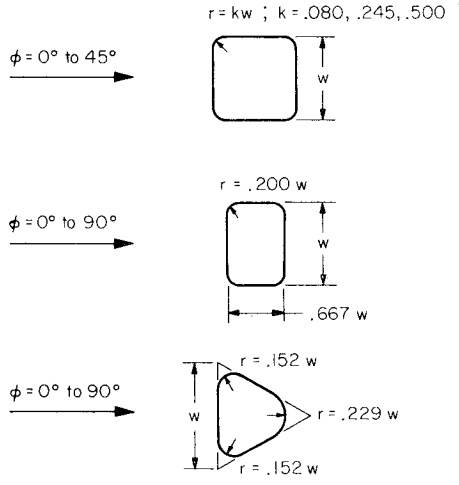
44 (Delany & Sorensen)	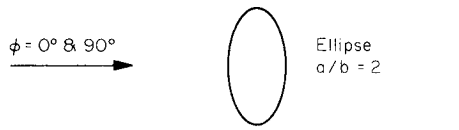

References	Cross sections and flow directions
44 (Delany & Sorensen)	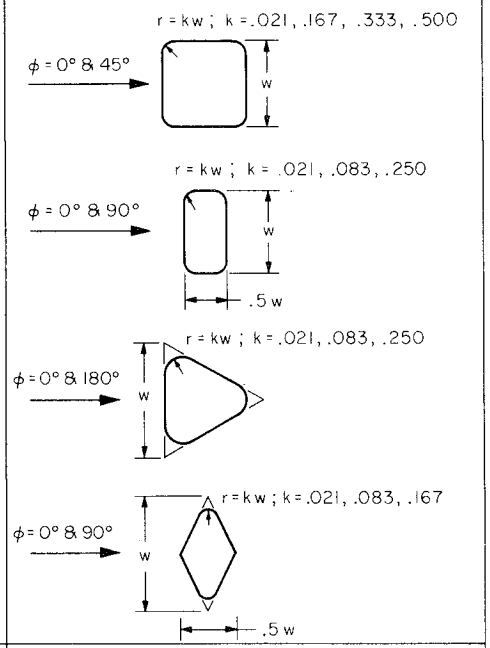
45 (Polhamus, Geller, & Grunwald)	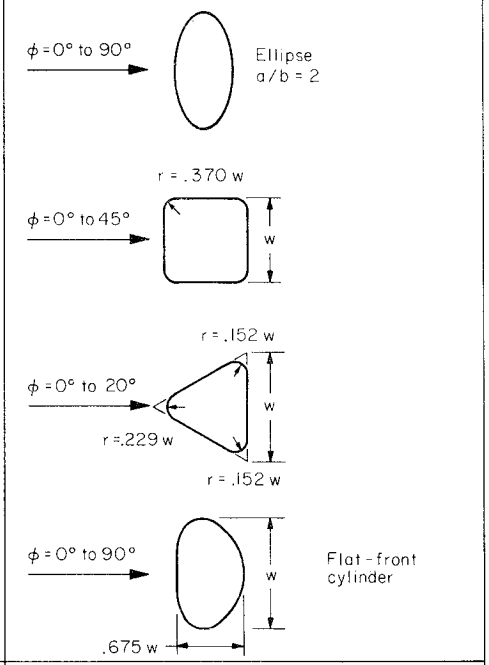
46 (Lockwood)	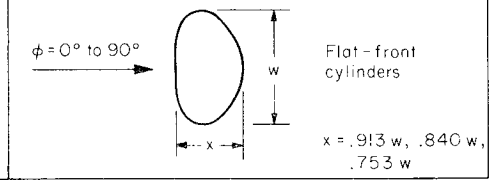

Axial-force coefficients – The same basic procedures and equations (eqs. (2), (3) and (9)) can be used to estimate the axial-force coefficients for bodies of noncircular cross section as for bodies of revolution. Because of lack of investigation, however, there is little information from which to compute the pressure contribution to the axial-force coefficients at α of 0° of 180°. For bodies with cross sections that are not too different from circular, the pressure axial-force coefficients might be roughly estimated by computing the coefficients for the equivalent body of revolution (circular body with the same axial distribution of cross-sectional area). This procedure was shown to give reasonable results in reference 9. More refinement in the computation procedure, however, is possible for cone-cylinder bodies with elliptic cross sections.

For conical-nosed bodies of elliptic cross section, the pressure axial-force coefficient at $\alpha = 0°$ has been derived by Van Dyke (ref. 47) from second-order slender-body theory. It is given by

$$C_{A_W} = a\,b\,(2\lambda+1) + \beta^2\,a\,b\left[3\,a\,b\lambda^2 + \frac{3}{2}(a^2+b^2)\,\lambda - \frac{1}{2}(a-b)^2 + \frac{1}{2}\,a\,b\right]$$

$$+ a^2\,b^2\left[(\gamma+1)\frac{M_\infty^4}{\beta^2} - (2+M_\infty^2)\,\lambda + \left(\frac{1}{4}\,M_\infty^2 - 1\right)\frac{a^2+b^2}{2\,a\,b}\right]$$

$$+ M_\infty^2\,a^2\,b^2\left[\frac{3}{8}\,\frac{a^2+b^2}{a\,b} - (\lambda+1) + \frac{3}{2}\,\frac{ab}{a^2-b^2}\log\,\frac{a}{b}\right] \tag{28}$$

where

$$\lambda = \log\frac{4}{\beta\,(a+b)} - 1\,, \quad \beta = \sqrt{M_\infty^2 - 1}$$

and a and b are slopes of the semimajor and semiminor axes.

For conical-nosed bodies of elliptic cross section, the skin-friction coefficient $C_{A_{SF}}$ at $\alpha = 0°$ can be computed by the same flat-plate skin-friction methods as for the bodies of revolution, but the wetted area of the noncircular body should be used. For an elliptic cone nose, the surface wetted area can be determined closely from

$$A_S \approx \pi\,(a+b)\,\frac{64-3\sigma^4}{64-16\sigma^2}\sqrt{\frac{a\,b+\ell_N^2}{2}} \tag{29}$$

where

$$\sigma = \frac{a-b}{a+b}$$

and a and b are the semimajor and semiminor axes.

COMPARISON OF COMPUTED WITH EXPERIMENTAL AERODYNAMIC CHARACTERISTICS FOR NINE BODIES OF REVOLUTION

Bodies Studied and Flow Conditions

The longitudinal aerodynamic characteristics for a series of cylinder, cone-cylinder, and ogive-cylinder bodies of revolution with various nose and afterbody fineness ratios were measured by Jernell (ref. 4) in the Langley Unitary Plan Wind Tunnel. Data were obtained for Mach numbers from 1.50 to 2.86, angles of attack from about $-5°$ to $180°$, and a Reynolds number based on diameter of 1.25×10^5.

Drawings of the bodies are shown in figure 9 along with values of the geometric parameters required to compute the aerodynamic characteristics. For the cylinder-only bodies (numbers 1 and 2)

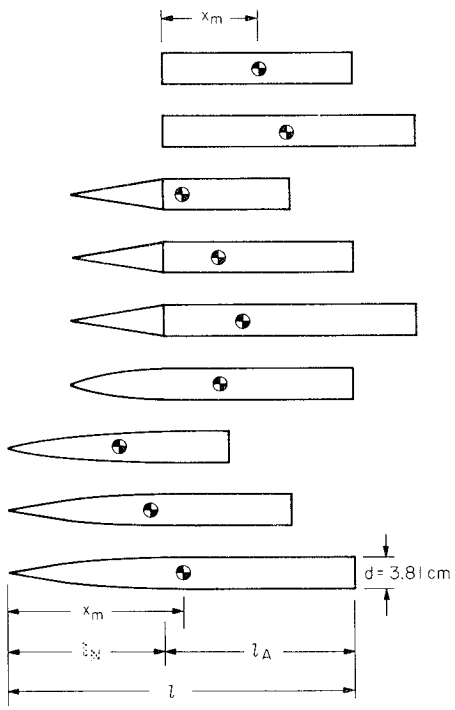

Body no.	$\frac{l}{d}$	$\frac{l_N}{d}$	$\frac{l_A}{d}$	$\frac{x_m}{d}$	$\frac{A_p}{d^2}$	$\frac{V}{d^3}$	$\frac{x_c}{d}$	$\frac{A_s}{d^2}$	Nose shape
1	6	0	6	3	6.000	4.710	3.000	19.63	Flat
2	8	0	8	4	8.000	6.280	4.000	25.92	Flat
3	7	3	4	3.5	5.500	3.925	4.183	17.34	Cone
4	9	3	6	4.5	7.500	5.495	5.200	23.62	Cone
5	11	3	8	5.5	9.500	7.065	6.211	29.91	Cone
6	9	3	6	4.5	8.011	5.977	4.963	25.24	Ogive
7	7	5	2	3.5	5.340	3.671	4.200	16.82	Ogive
8	9	5	4	4.5	7.340	5.241	5.234	23.10	Ogive
9	11	5	6	5.5	9.340	6.811	6.255	29.38	Ogive

Figure 9. – Bodies for which the aerodynamic characteristics were measured in reference 4 and computed in the present study for $M_\infty = 2.86$.

and cone-cylinder bodies (numbers 3-5) all of these geometric parameters are easily computed, but for the bodies with tangent-ogive noses (numbers 6-9) the values of A_p/d^2, V/d^3, x_c/d, and A_s/d^2 are not so easily obtained. Some convenient formulas for computing these parameters for tangent-ogive noses are given in the appendix.

In the present study the aerodynamic characteristics for the bodies shown in figure 9 have been computed only for $M_\infty = 2.86$. Jernell (ref. 4) found appreciable discontinuities in his data, believed to be due primarily to interference effects from the model support system, as evidenced by schlieren photographs. Although these data discontinuities persist throughout the test Mach number range from 1.50 to 2.86, they appear to diminish slightly with increase in Mach number. The data for $M_\infty = 2.86$ are probably the least affected by interference, and for this reason computed results are compared only with these data. Also, because of interference effects, any trends in the experimental aerodynamic characteristics with change in Mach number from only 1.50 to 2.86 may be erroneous.

The procedure outlined in this report has been used to compute the variation of C_N, C_A, C_m, and x_{ac}/ℓ with α for the nine bodies of figure 9 at $M_\infty = 2.86$. Turbulent boundary layer flow and zero heat transfer were assumed because Jernell (ref. 4) states that "boundary-layer transition was effected" by artificial trips throughout the α range.

Variation of C_N, C_A, and C_m With Angle of Attack

In figures 10 through 14, computed values of C_N, C_A, and C_m as a function of angle of attack α are compared with the experimental results for the nine bodies at $M_\infty = 2.86$. Generally there is good agreement of the computed with the measured results, especially in the variation of C_N and C_m with α. The poorest agreement is between values of C_A, and further comment on this disparity will be made shortly.

It is gratifying that effects of afterbody fineness ratio, nose fineness ratio, and nose shape on C_N and C_m are predicted so well. In general the magnitudes of C_N and C_m increase with increase in fineness ratio, just as the computed results predict. Figure 10 shows the effect of fineness ratio for flat-nosed cylinders. Figure 11 shows the effect of fineness ratio for cone-cylinder bodies, all with fineness ratio 3 conical noses. Likewise, figure 12 shows the effect of fineness ratio for ogive-cylinder bodies, all with fineness ratio 5 ogival noses. Figure 13 shows the effect of nose fineness ratio for ogive-cylinder bodies, and figure 14 shows the effect of change in nose shape from conical to ogival for a given fineness ratio.

It is believed that at least some of the disagreement between computed and measured values of C_A can be attributed to support interference effects. No adjustments were made in the data of reference 4 for base-pressure conditions, and the coefficients represent total measured axial force. It is not understood why there is such a significant increase in measured C_A for the conical- and ogival-nosed bodies as α increases from 0° to about 70° (figs. 11-14). The measured values of C_A pass through zero at an α above $\alpha = 90°$, probably in part because of different spillage flow around the nose than the base of each model. Here again, however, there is evidence of support interference, since the C_A values for the flat-faced cylinders (bodies 1 and 2) also pass through zero at an α a little above $\alpha = 90°$ (see fig. 10).

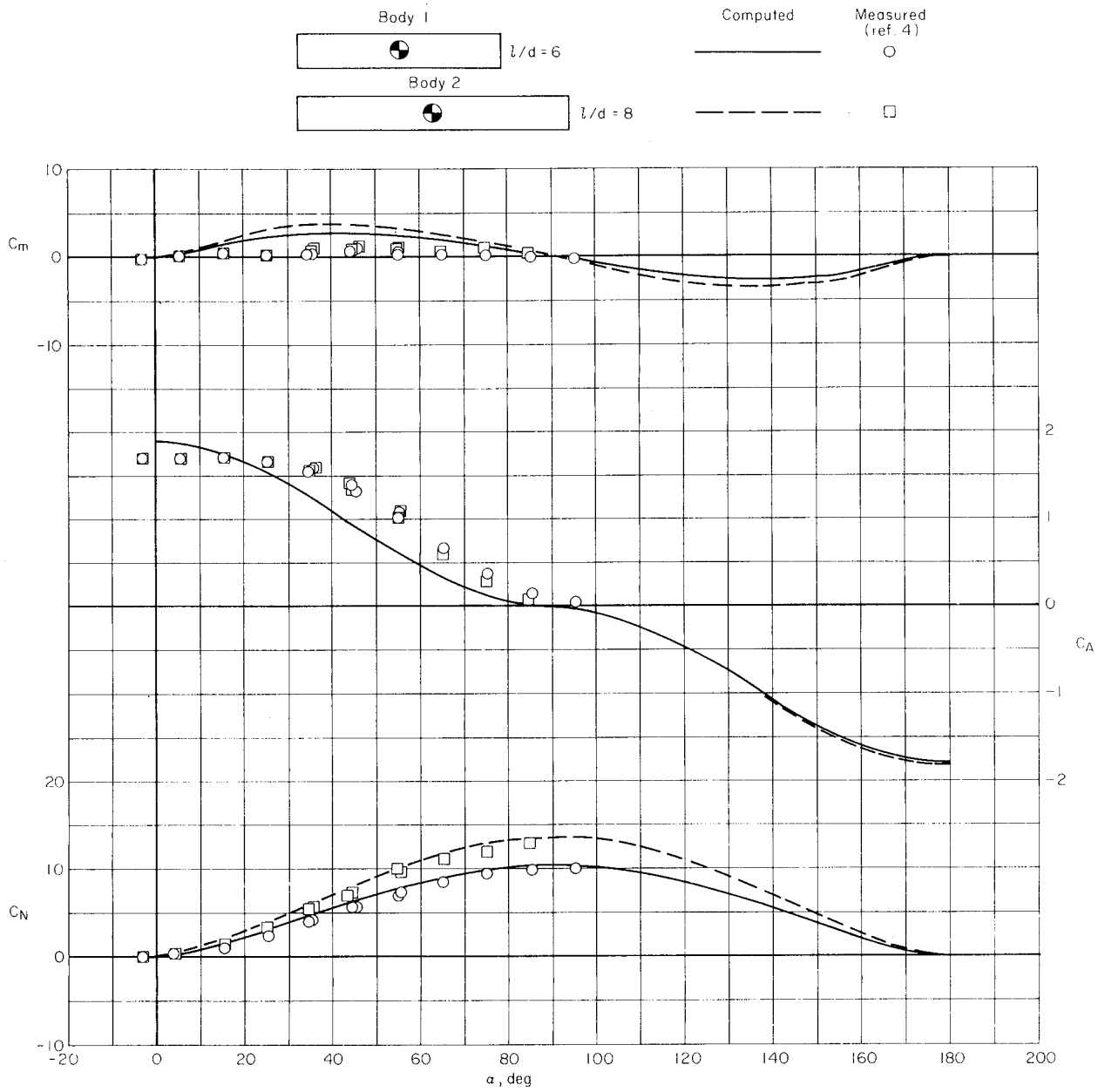

Figure 10. – Comparison of computed with measured aerodynamic characteristics for cylindrical bodies with completely blunt noses; $M_\infty = 2.86$.

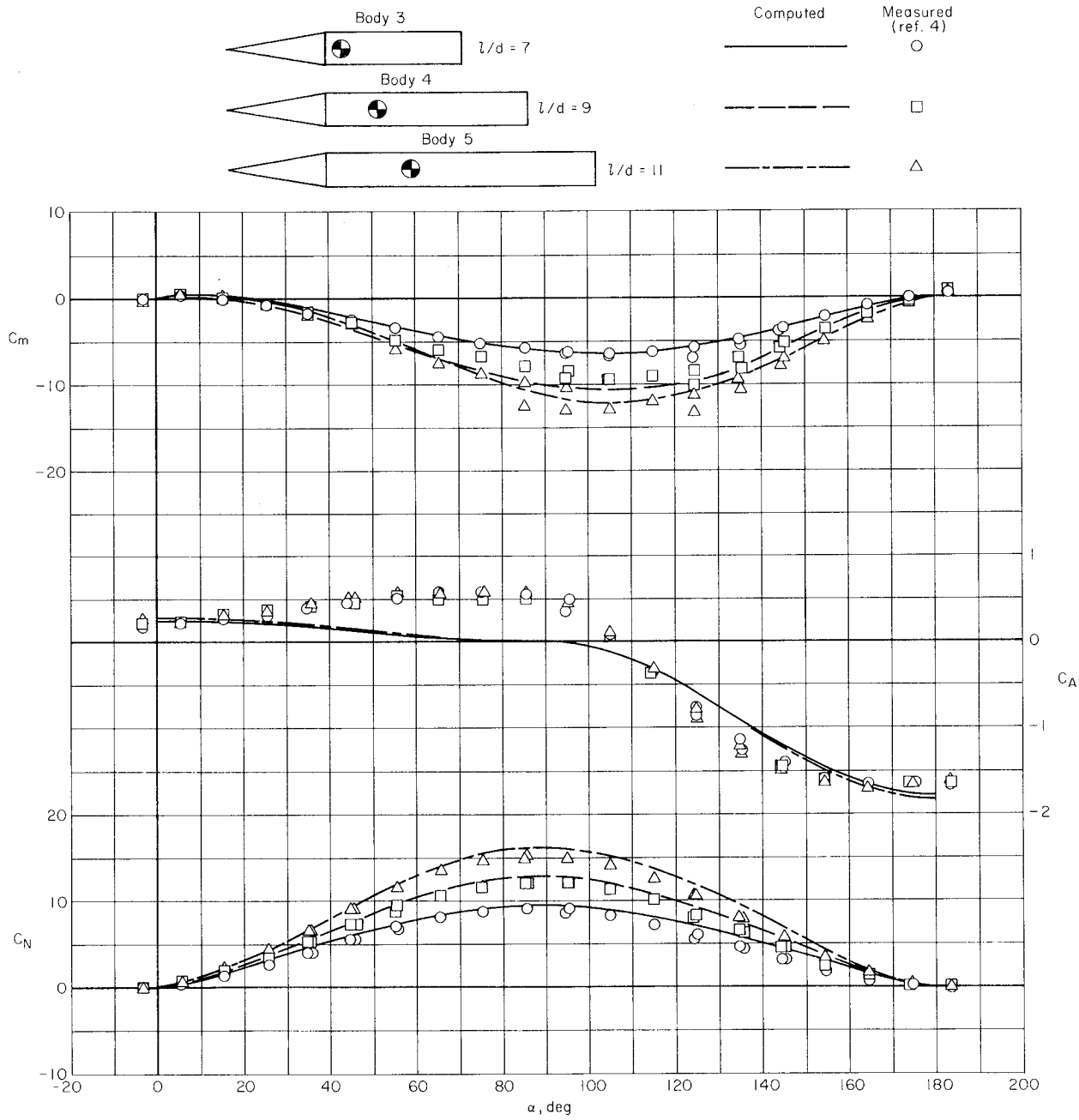

Figure 11. – Comparison of computed with measured aerodynamic characteristics for cylindrical bodies with conical noses of fineness ratio 3; $M_\infty = 2.86$.

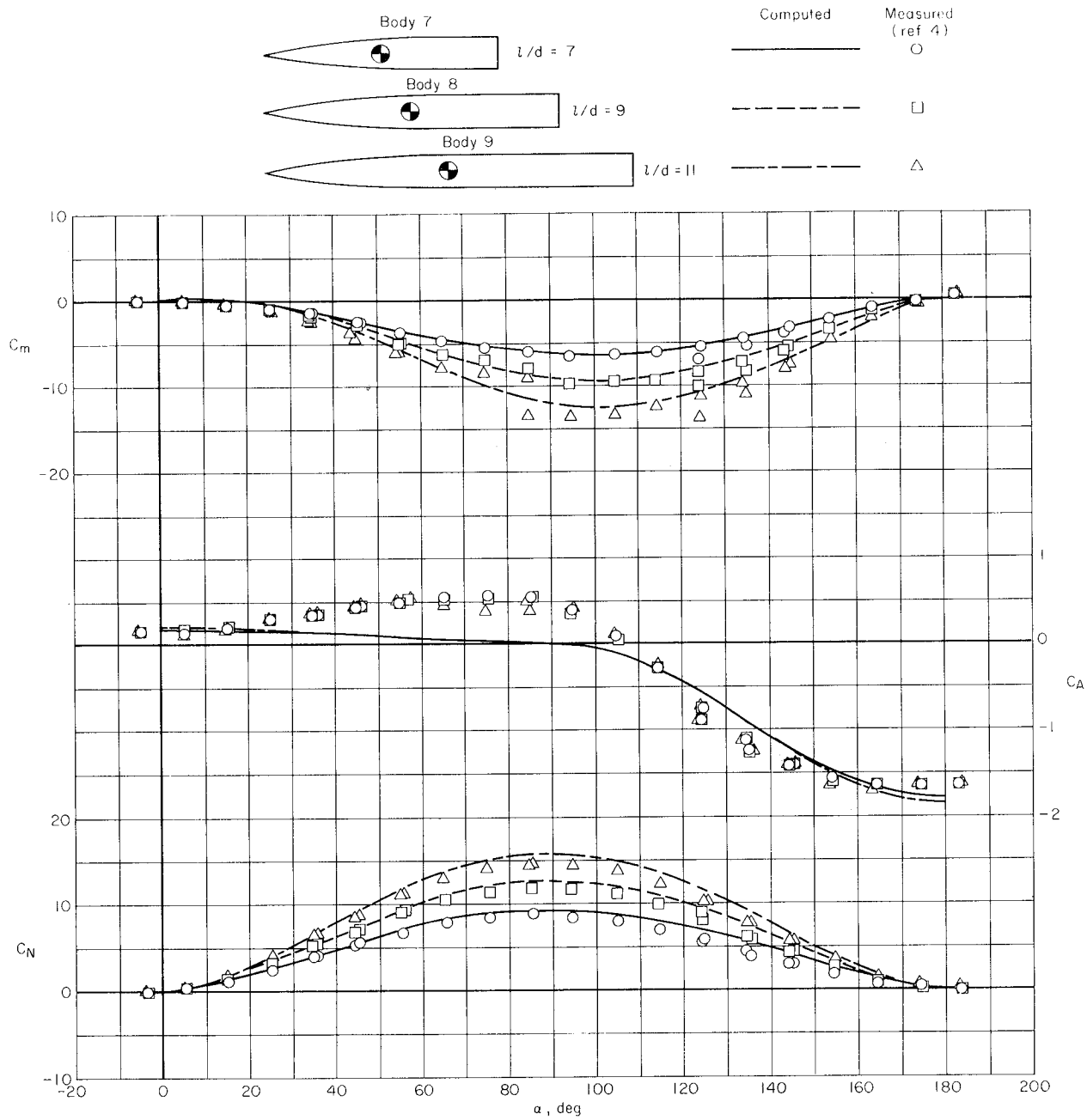

Figure 12. – Comparison of computed with measured aerodynamic characteristics for cylindrical bodies with ogival noses of fineness ratio 5; $M_\infty = 2.86$.

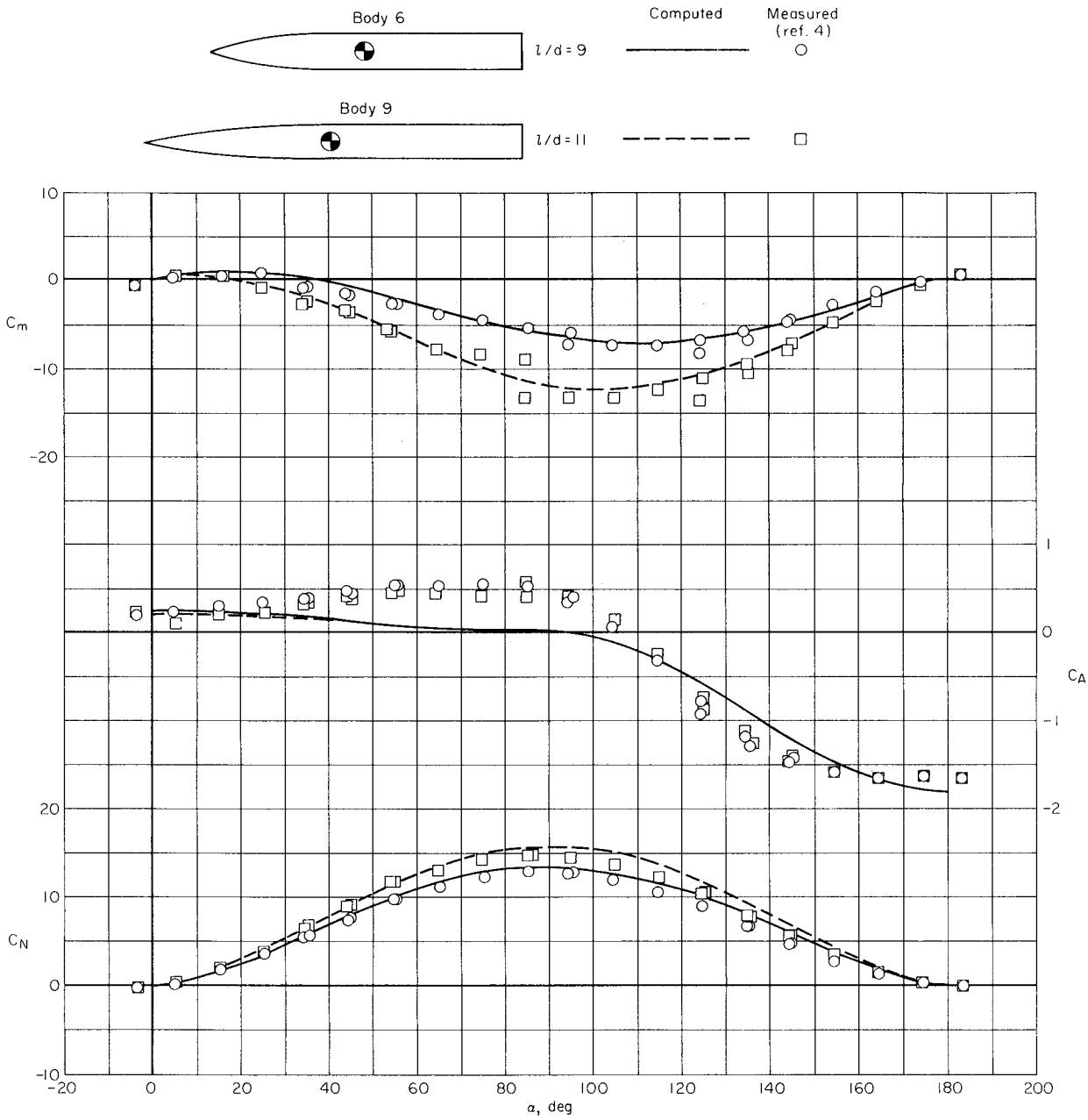

Figure 13. – Comparison of computed with measured aerodynamic characteristics for cylindrical bodies with ogival noses of fineness ratio 3 and 5; $M_\infty = 2.86$.

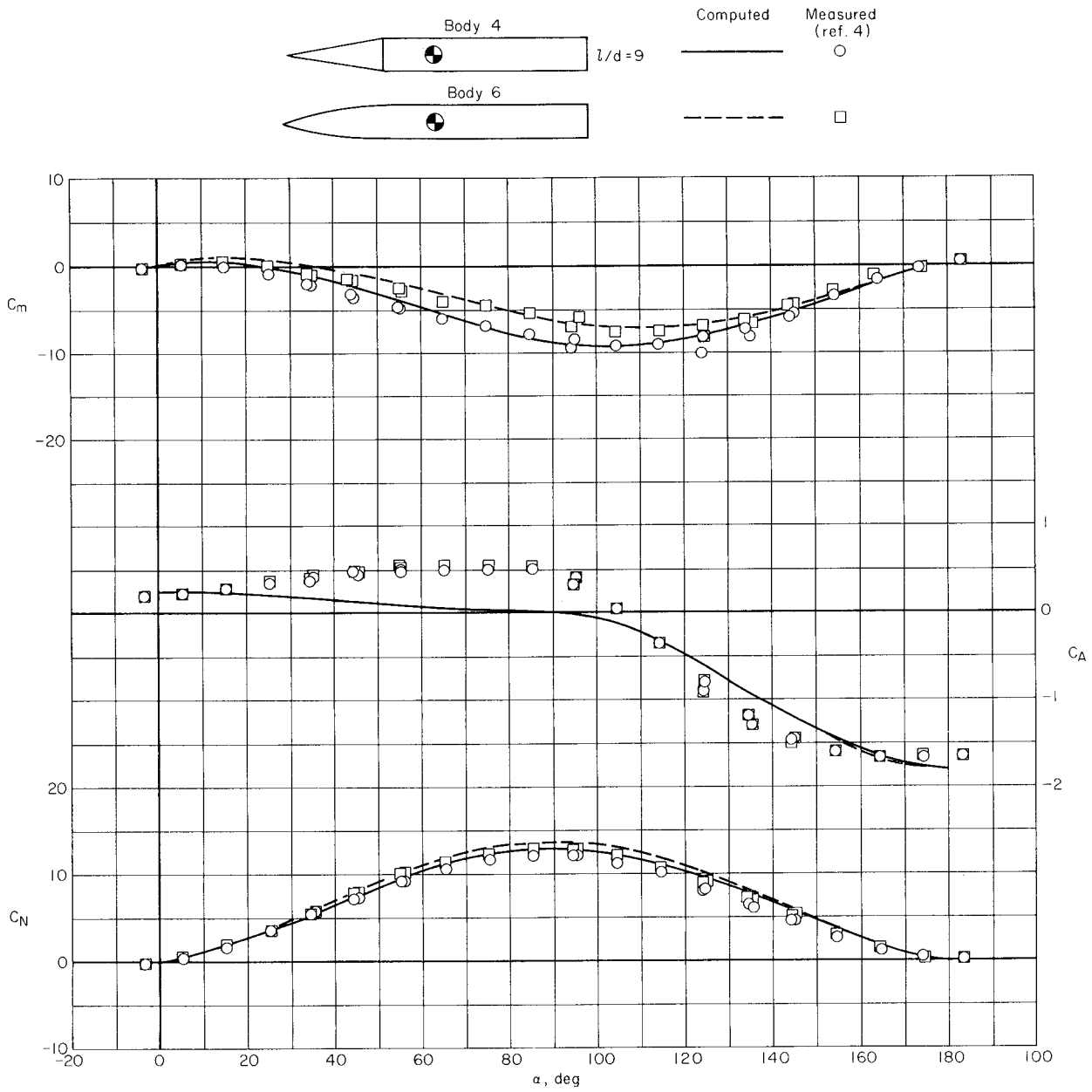

Figure 14. – Comparison of computed with measured aerodynamic characteristics for cylindrical bodies with conical and ogival noses of fineness ratio 3; $M_\infty = 2.86$.

Equations (2) and (3) were used to compute the variation of C_A with α, and the values include the contributions of fore pressure, turbulent skin friction, and base pressure. Although no attempt was made to compute the magnitude of wind-tunnel support interference, additional values of C_A for body number 5, a cone-cylinder, were computed by the alternate, more precise, method previously outlined.

In figure 15, C_A's computed by both methods are compared with the measured values for body number 5. It is seen that use of the more precise method (the dashed line) only slightly changes the comparison of computed with measured results. Also, the variation of C_A with α by the more precise method is limited to α's less than 69.5°. This limitation results from the fact that $M_a < 1$ for $\alpha > 69.5°$ with $M_\infty = 2.86$, and supersonic cone theory for determining C_{a_W} is not applicable. In the computations, C_{a_W} values for the conical nose were determined with the use of equation (10), the cone tables in reference 48, and chart 6 in reference 31. Computed C_A results with and without base pressure (from eq. (11)) are shown for comparison in figure 15.

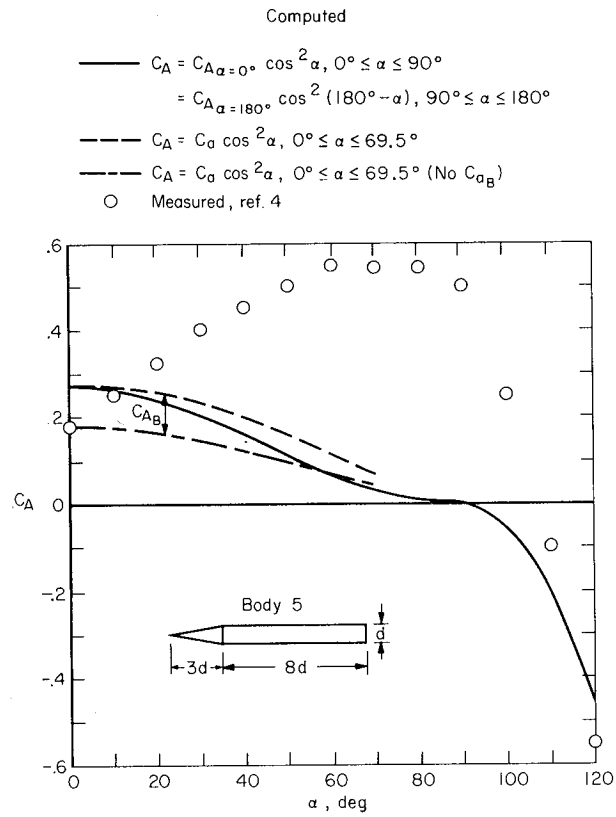

Figure 15. – Comparison of computed axial-force coefficients with measured axial-force coefficients for a cone-cylinder body (body 5); $M_\infty = 2.86$.

Variation of x_{ac}/ℓ With Angle of Attack

In figure 16 computed values of aerodynamic force center (the symbols) are compared with the experimental results (the lines from ref. 4) for the nine bodies at $M_\infty = 2.86$. As for the C_N and C_m results, the agreement of the computed with the measured values is reasonably good, especially for α near 90°. Note that symbols are used to denote computed values because lines are used in reference 4 to denote the measured results. At α somewhat less than and greater than 90°, the computed values are generally a little forward of the measured values. The greatest differences between predicted and measured results occur with the blunt cylindrical portions of the bodies almost facing into the free-stream flow (i.e., for α approaching 0° and 180° for the completely blunt-nosed bodies and α approaching 180° for the pointed-nosed bodies).

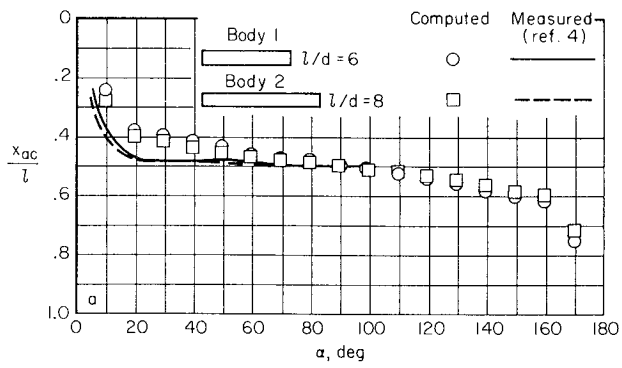

(a) Cylindrical bodies with completely blunt noses.

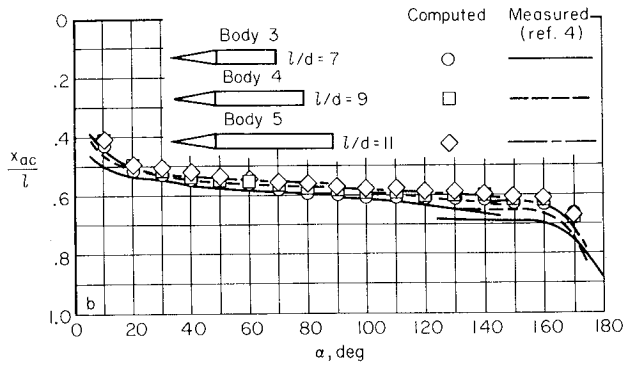

(b) Cylindrical bodies with conical noses of fineness ratio 3.

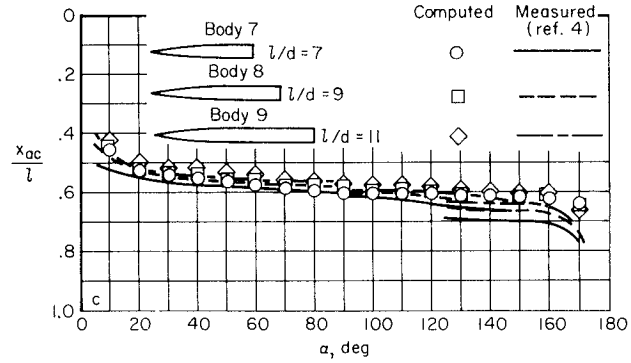

(c) Cylindrical bodies with ogival noses of fineness ratio 5.

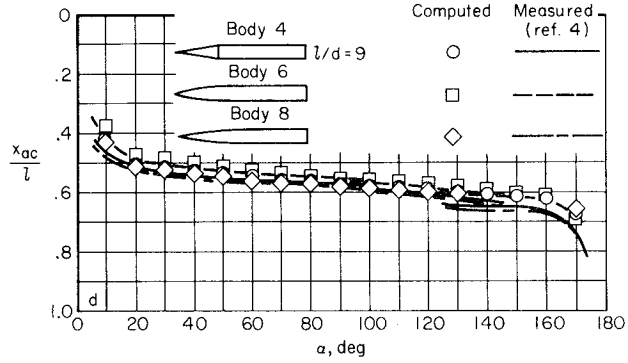

(d) Cylindrical bodies with conical and ogival noses.

Figure 16. – Comparison of computed with measured aerodynamic force centers for cylindrical bodies with completely blunt noses, with conical noses, and with ogival noses; $M_\infty = 2.86$.

PREDICTED EFFECTS OF MACH NUMBER AND REYNOLDS NUMBER ON BODY AERODYNAMIC CHARACTERISTICS

The procedure reviewed in this report has been used to predict some effects of Mach number and Reynolds number on the variation of C_N and x_{ac}/ℓ with α for a body of revolution. The body consists of a fineness ratio 5 ogival nose followed by a fineness ratio 6 cylinder (body number 9 in fig. 9). It is believed that the aerodynamic trends computed for this body are indicative of those that can be expected for most booster bodies at comparable Mach numbers, Reynolds numbers, and angles of attack.

Effect of Mach Number

The variation of C_N and x_{ac}/ℓ with α has been computed for several free-stream Mach numbers from hypersonic down to subsonic ($M_\infty = 7.0$, 2.9, 1.5, and 0.3), and the curves are presented in figure 17. It is seen that Mach number significantly affects C_N over most of the α range. The aerodynamic force center, however, moves little with change in Mach number.

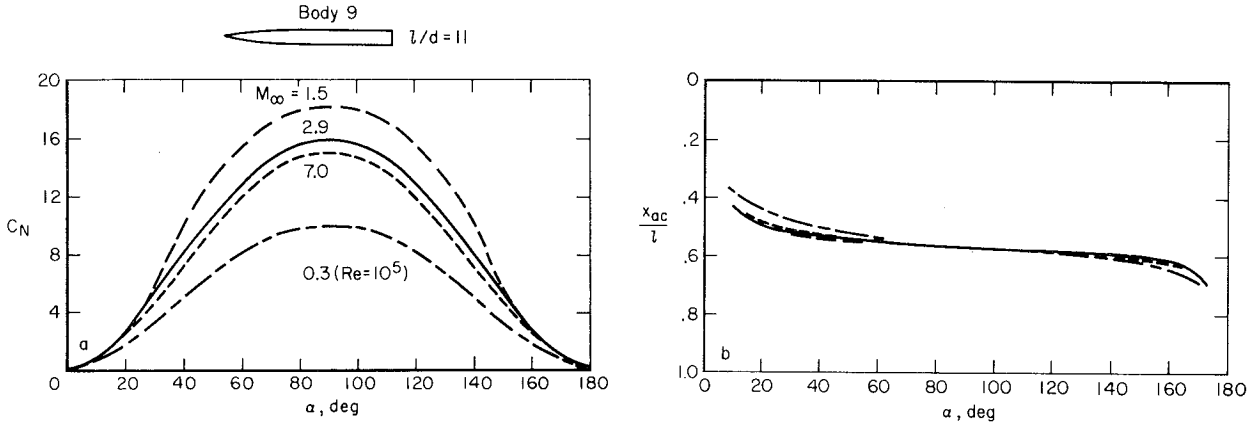

(a) Normal force coefficients.

(b) Aerodynamic force centers.

Figure 17. – Effect of Mach number on the computed aerodynamic characteristics of an ogive-cylinder body.

Naturally, because of the semiempirical method used, the C_N curves, especially at α near $\alpha = 90°$, strongly reflect the variation of crossflow drag coefficient C_{d_n} with crossflow Mach number M_n for two-dimensional circular cylinders (see fig. 1). That is, as M_∞ decreases from $M_\infty = 7.0$ to $M_\infty = 1.5$ (fig. 17), C_N increases as does C_{d_n}. Although the transonic crossflow Mach number range is not well defined for two-dimensional circular cylinders, C_{d_n} probably reaches a maximum at or near $M_n = 1$ (fig. 1), and the computed C_N for a booster body would reach a maximum at or near $M_\infty = 1$ with $\alpha = 90°$ (since $M_n = M_\infty \sin \alpha$). As the free-stream Mach number decreases to low subsonic ($M_\infty \lesssim 0.3$), there is considerable drop in maximum C_{d_n} and, hence, in computed C_N. See, for example, the C_N curve for $M_\infty = 0.3$ in figure 17.

It should be noted that the C_N curve for $M_\infty = 0.3$ was computed for a free-stream Reynolds number of $Re = 10^5$, so that, throughout the α range, all of the values of crossflow Reynolds number ($Re_n = Re \sin \alpha$) are subcritical and $C_{d_n} \simeq 1.2$ (see fig. 2). The topic next discussed is the effect on C_N and x_{ac}/ℓ of increasing Re above $Re = 10^5$ so that values of Re_n lie within the supercritical range.

Effect of Reynolds Number

For M_∞ less than about 0.4, the variation of C_N and x_{ac}/ℓ with α has been computed for free-stream Reynolds numbers of 10^5, 10^6, and 10^7, and the curves are presented in figure 18. It is seen

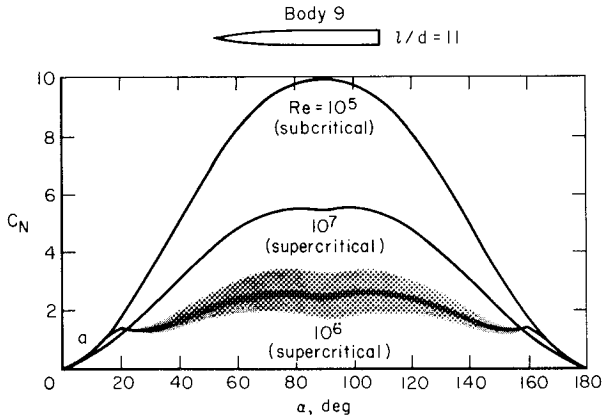

(a) Normal force coefficients.

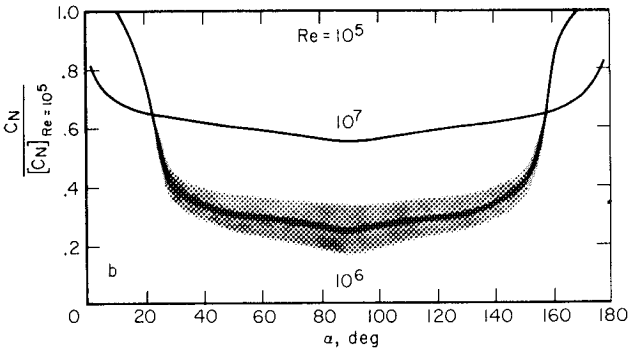

(b) Ratios of normal force coefficients.

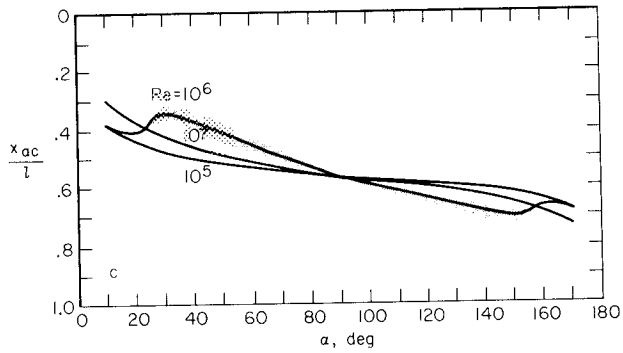

(c) Aerodynamic force centers.

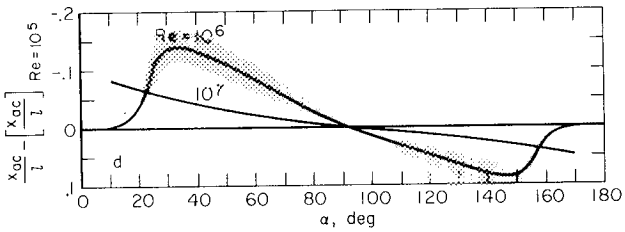

(d) Differences between aerodynamic force centers.

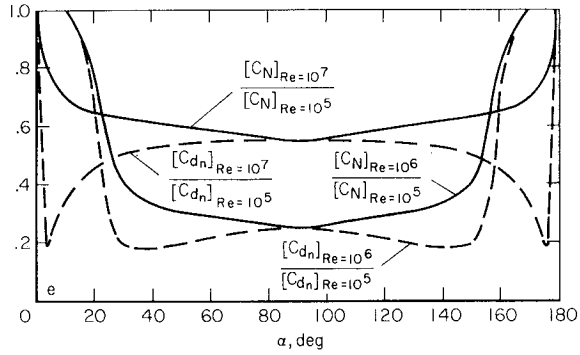

(e) Comparisons of ratios of normal force coefficients with ratios of crossflow drag coefficients.

Figure 18. – Effect of supercritical Reynolds numbers on the computed aerodynamic characteristics of an ogive-cylinder body at subcritical crossflow Mach numbers ($M_n \lesssim 0.4$).

that there is a significant effect of Reynolds number on both C_N and x_{ac}/ℓ throughout most of the α range. These curves, of course, reflect the strong influence of crossflow Reynolds number Re_n on crossflow drag coefficient C_{d_n} for two-dimensional circular cylinders (see fig. 2).

As shown in figure 2, C_{d_n} for a circular cylinder drops considerably as Re_n increases from 10^5 to 10^6, and then there is gradual rise as Re_n increases from 10^6 to 10^7. There apparently is much more uncertainty in the magnitude of C_{d_n} at supercritical Re_n (such as 10^6 and 10^7) than at subcritical Re_n (values less than about 2×10^5), and the shading in figure 2 indicates the uncertainty because of scatter in known data.

In figure 18 the shaded bands in the C_N and x_{ac}/ℓ curves for $Re = 10^6$ reflect the uncertainty in these curves resulting from the scatter in the C_{d_n} data shown in figure 2. It is clearly evident, however, that this uncertainty in the curves is relatively small compared with the large effect of change in Reynolds number.

In figure 18(b) is shown the ratio of C_N for the body at Re of 10^6 and 10^7 to C_N for the body at the subcritical Re of 10^5. With this figure, the effect of Re can be studied throughout the α range. It is seen, for example, that at α near 90° the body at $Re = 10^6$ develops only about 25 percent of the C_N developed at $Re = 10^5$, but at α less than about 10°, 100 percent of the C_N is developed. Similar study in the movement of x_{ac}/ℓ with change in Re and α can be made with the use of figures 18(c) and (d).

The curves in figure 18(e) verify that quick estimates of $C_N/\left[C_N\right]_{Re = 10^5}$ can be made for α from about 60° to 120° by assuming that

$$\frac{C_N}{\left[C_N\right]_{Re = 10^5}} \approx \frac{C_{d_n}}{\left[C_{d_n}\right]_{Re = 10^5}}$$

Values of C_{d_n} for Re of interest can be readily read from figures 2 and 3.

Verification of Effect of Reynolds Number from Experimental Data

Experimental results have been obtained (ref. 3) which show significant effects of Reynolds number and body corner radius on the force and moment characteristics of a flat-bottomed space-shuttle-type model at high angles of attack and at low subsonic Mach numbers ($M_\infty \simeq 0.3$). A sampling of C_N data from reference 3 for a given corner radius is plotted in figure 19. These data show a large effect of Reynolds number (based on body width) on the variation of $(A/A_p)C_N$ with α over the α range investigated ($35° \leq \alpha \leq 75°$).

Reference 3 shows that there is close similarity, in both magnitude and change with Reynolds number, between the crossflow drag coefficients for this shuttle body at high α and two-dimensional square cylinders with rounded corners at 90° angle of attack. From this similarity it is concluded

that these data lie within the critical Reynolds number range, the range in which the crossflow drag coefficient decreases from high to low values as the Reynolds number increases from subcritical to critical.

With the use of plots of C_{d_n} versus Re_n for two-dimensional square cylinders with various corner radii (fig. 6 in ref. 3), normal-force coefficients have been computed for the shuttle body and are compared with the data in figure 19. Although the computed results do not agree closely with the measured, they do qualitatively predict the significant effect of Reynolds number.

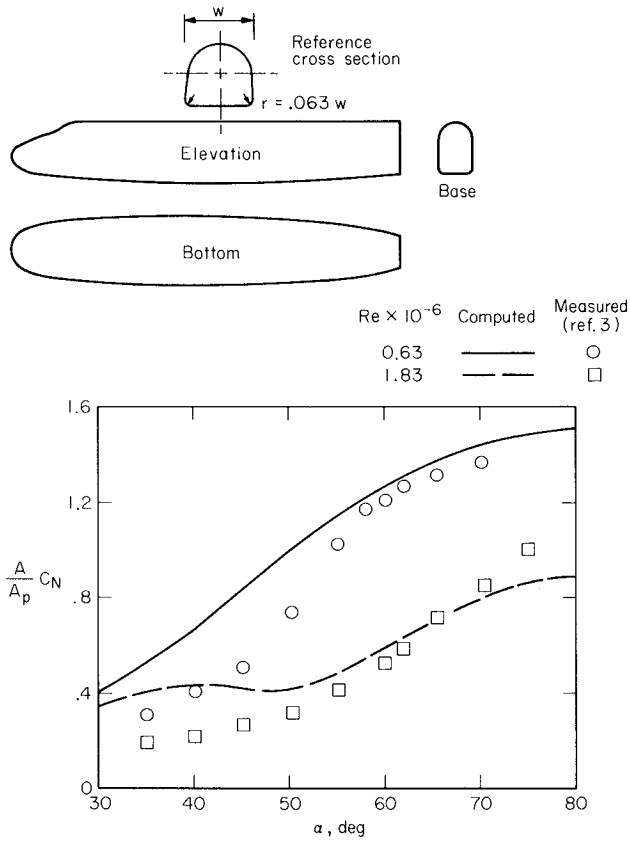

Figure 19. – Comparison of computed with measured effect of Reynolds number on variation of normal-force coefficient with angle of attack for a space shuttle-type body (flat bottomed with rounded corners) at $M_\infty = 0.3$.

In addition to the somewhat explainable C_N and C_m results measured in reference 3 for this shuttle body, sideslip results were measured that are difficult to understand and, at present, impossible to predict. It is believed, however, that they are associated with body boundary-layer-flow separation and vortex action – particularly the phenomenon that includes unsymmetrical boundary-layer separation, unsymmetrical vortex formation, and random switching of vortex position with time which has been observed for bodies at high angles of attack.

It is hoped that the very limited results in reference 3 and in this report will serve as a "red warning flag" concerning possible uncertainties and unpredictable aerodynamic effects for shuttle boosters and missiles at subcritical crossflow Mach numbers and supercritical crossflow Reynolds numbers. If shuttle boosters are to be flown back into the atmosphere at very high angles of attack to low subsonic Mach numbers, further effort should be made to obtain detailed wind-tunnel data at near-flight Reynolds numbers.

CONCLUDING REMARKS

The following remarks are written to correspond with the three study objectives stated in the Introduction.

(1) An engineering-type procedure with formulas and plots has been presented for computing normal force, axial force, and pitching-moment coefficients for booster-like bodies of circular and various noncircular cross sections. Included are necessary "state-of-the knowledge" plots of circular-

cylinder crossflow drag coefficient versus crossflow Mach number and crossflow Reynolds number. Some available plots of crossflow drag coefficient versus crossflow Reynolds number for various non-circular cross sections are referenced.

(2) The presented procedure has been used to predict the variation of C_N, C_A, C_m, and x_{ac}/ℓ with α for nine bodies of revolution at $M_\infty = 2.86$. Except for C_A, the agreement of the predicted with the available measured results is good throughout the α range.

(3) Effects of Mach number and Reynolds number on the variation of C_N and x_{ac}/ℓ with α have been predicted for a body of revolution (fineness ratio 5 ogival nose with a fineness ratio 6 cylinder aftersection). Mach number changes from $M_\infty = 7$ down to $M_\infty = 0.3$ (the range studied) can significantly affect C_N over most of the α range. The aerodynamic force center, however, moves little with Mach number.

Even more pronounced than the effect of Mach number is the effect of Reynolds number, which has been predicted for the body at the subcritical Mach number of $M_\infty \simeq 0.3$. With increase in Reynolds number from 10^5 to 10^6, up to 75 percent of the normal force is lost, the maximum loss occurring at $\alpha = 90°$. With further increase in Reynolds number to $Re = 10^7$, only about one-half of the normal force at $Re = 10^5$ is regained. This large effect of Reynolds number results from the fact that the crossflow Reynolds numbers vary from subcritical to critical as freestream Reynolds number increases well above $Re = 10^5$.

The fact that there can be a severe effect of Reynolds number on the aerodynamics when the crossflow Reynolds numbers are in the critical range also has been demonstrated with experimental results for a flat-bottomed shuttle-type body. Computed normal-force coefficients for this body at $M_\infty = 0.3$ qualitatively predict the significant measured effect of changing the crossflow Reynolds number through the critical range.

The results of this investigation suggest that, if shuttle boosters (and other vehicles) are to be flown back into the atmosphere at very high angles of attack to low subsonic Mach numbers, effort should be made to obtain wind-tunnel data at near flight Reynolds numbers.

Ames Research Center
National Aeronautics and Space Administration
Moffett Field, California, August 9, 1972

APPENDIX

FORMULAS TO COMPUTE GEOMETRIC PARAMETERS FOR TANGENT OGIVES

To compute the aerodynamic characteristics of bodies of revolution having tangent ogive nose shapes, various geometric parameters must be obtained. To compute C_N and C_m the planform area A_p is required, and to compute C_m it is also necessary to obtain the volume V and the distance x_c from the nose vertex to the centroid of planform area. To compute skin-friction drag, the wetted surface area A_s is needed.

For an ogival nose of length ℓ_N and diameter d (see sketch (e)) the following useful formulas have been derived:

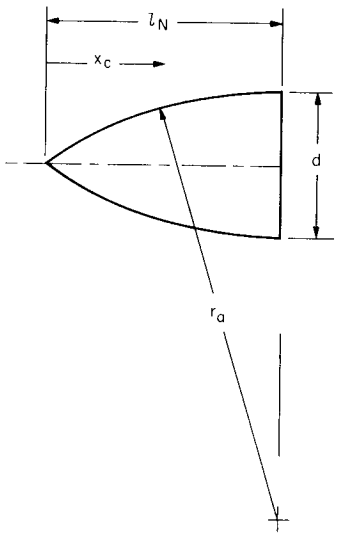

Sketch (e)

$$\frac{A_p}{d^2} = \frac{\ell_N}{d}\sqrt{R^2 - \left(\frac{\ell_N}{d}\right)^2} + R^2 \sin^{-1}\left(\frac{\ell_N/d}{R}\right) - 2\left(\frac{\ell_N}{d}\right)\left(R - \frac{1}{2}\right) \tag{A1}$$

$$\frac{V}{d^3} = \pi\left[\frac{2}{3}\left(\frac{\ell_N}{d}\right)^3 - \frac{A_p}{d^2}\left(R - \frac{1}{2}\right)\right] \tag{A2}$$

$$\frac{x_c}{d} = \frac{\ell_N}{d} - \frac{\frac{2}{3}\left\{R^3 - \left[R^2 - \left(\frac{\ell_N}{d}\right)^2\right]^{3/2}\right\} - \left(\frac{\ell_N}{d}\right)^2\left(R - \frac{1}{2}\right)}{\frac{A_p}{d^2}} \tag{A3}$$

and

$$\frac{A_s}{d^2} = 2\pi R\left[\left(R - \frac{1}{2}\right)\sin^{-1}\left(\frac{-\ell_N/d}{R}\right) + \frac{\ell_N}{d}\right] \tag{A4}$$

where R is the ratio of the ogival arc radius r_a to base diameter d, and

$$R = \frac{r_a}{d} = \left(\frac{\ell_N}{d}\right)^2 + \frac{1}{4}$$

REFERENCES

1. Peterson, Victor L.; Katzen, Elliott D.; Axelson, John A.; Brownson, Jack J.; Cliffone, Donald L.; Cleary, Joseph W.; Intrieri, Peter F.; Malcolm, Gerald N.; and Mellenthin, Jack A.: Static and Dynamic Aerodynamics of Space Shuttle Vehicles. Presented at NASA Space Shuttle Technology Conference, March 2-4, 1971, pp. 311-373. NASA TM X-2272, 1971.

2. Hamilton, Richard K.: Correlation of Space Shuttle Applicable Experimental Hypersonic Aerodynamic Charistics with Theory. Presented at NASA Space Shuttle Technology Conference, March 2-4, 1971, pp. 455-492. NASA TM X-2272, 1971.

3. Jorgensen, Leland H.; and Brownson, Jack J.: Effects of Reynolds Number and Body Corner Radius on Aerodynamic Characteristics of a Space Shuttle-Type Vehicle at Subsonic Mach Numbers. NASA TN D-6615, 1972.

4. Jernell, Lloyd S.: Aerodynamic Characteristics of Bodies of Revolution at Mach numbers from 1.50 to 2.86 and Angles of Attack to 180°. NASA TM X-1658, 1968.

5. Allen, H. Julian: Estimation of the Forces and Moments Acting on Inclined Bodies of Revolution of High Fineness Ratio. NACA RM A9I26, 1949.

6. Allen, H. Julian; and Perkins, Edward W.: A Study of Effects of Viscosity on Flow Over Slender Inclined Bodies of Revolution. NACA Rep. 1048, 1951.

7. Perkins, Edward W.; and Kuehn, Donald M.: Comparison of the Experimental and Theoretical Distributions of Lift on a Slender Inclined Body of Revolution at $M = 2$. NACA RM A53E01, 1953.

8. Perkins, Edward W.; and Jorgensen, Leland H.: Comparison of Experimental and Theoretical Normal-Force Distributions (Including Reynolds Number Effects) on an Ogive-Cylinder Body at Mach Number 1.98. NACA TN 3716, 1956.

9. Jorgensen, Leland H.: Inclined Bodies of Various Cross Sections at Supersonic Speeds. NASA MEMO 10-3-58A, 1958.

10. Lindsey, W. F.: Drag of Cylinders of Simple Shapes. NACA Rep. 619, 1938.

11. Stack, John: Compressibility Effects in Aeronautical Engineering. NACA ACR, 1941.

12. Gowen, Forrest E.; and Perkins, Edward W.: Drag of Circular Cylinders for a Wide Range of Reynolds Numbers and Mach Numbers. NACA TN 2960, 1953.

13. Walter, L. W.; and Lange, A. H.: Surface Temperature and Pressure Distributions on a Circular Cylinder in Supersonic Cross-Flow. NAVORD Rep. 2854 (Aeroballistic Res. Rep. 180), U.S. Naval Ord. Lab. (White Oak, Md.), June 5, 1953.

14. Penland, Jim A.: Aerodynamic Characteristics of a Circular Cylinder at Mach Number 6.86 and Angles of Attack up to 90°. NACA TN 3861, 1957.

15. Welsh, Clement J.: The Drag of Finite-Length Cylinders Determined From Flight Tests at High Reynolds Numbers for a Mach Number Range From 0.5 to 1.3. NACA TN 2941, 1953.

16. Relf, E. F.: Discussion of the Results of Measurements of the Resistance of Wires, with Some Additional Tests on the Resistance of Wires of Small Diameter. R. & M. No. 102, British A.C.A., 1914.

17. Wieselsberger, C.: New Data on the Laws of Fluid Resistance. NACA TN 84, 1922.

18. Polhamus, Edward C.: Effect of Flow Incidence and Reynolds Number on Low-Speed Aerodynamic Characteristics of Several Noncircular Cylinders With Applications to Directional Stability and Spinning. NASA TR R-29, 1959.

19. Roshko, Anatol: Experiments on the Flow Past a Circular Cylinder at Very High Reynolds Numbers. J. Fluid Mech., vol. 10, pt. 3, May 1961, pp. 345-356.

20. Schmidt, Louis V.: Fluctuating Force Measurements Upon a Circular Cylinder at Reynolds Numbers up to 5×10^6. Presented at Meeting on Ground Wind Load Problems in Relation to Launch Vehicles (Langley Research Center), June 7-8, 1966. NASA TM X-57,779, 1966.

21. Jones, George W., Jr.; Cinotta, Joseph J.; and Walker, Robert W.: Aerodynamic Forces on a Stationary and Oscillating Circular Cylinder at High Reynolds Numbers. NASA TR R-300, 1969.

22. Goldstein, Sydney.: Modern Developments in Fluid Dynamics. Oxford, The Clarendon Press, vol. 2, sec. 195, 1938, pp. 439-440.

23. McKinney, Linwood W.: Effects of Fineness Ratio and Reynolds Number on the Low-Speed Crosswind Drag Characteristics of Circular and Modified-Square Cylinders. NASA TN D-540, 1960.

24. Jorgensen, Leland H.; and Treon, Stuart L.: Measured and Estimated Aerodynamic Characteristics for a Model of a Rocket Booster at Mach Numbers from 0.6 to 4 and at Angles of Attack From 0° to 180°. NASA TM X-580, 1961.

25. Linnell, Richard D.; and Bailey, Jerry Z.: Similarity-Rule Estimation Methods for Cones and Parabolic Noses. Jour. Aero. Sci., vol. 23, no. 8, Aug. 1956, pp. 796-797.

26. Wittliff, Charles E.: Correlation of Drag Coefficients for Sharp Cones. AIAA J., vol. 6, no. 7, July 1968, pp. 1430-1431.

27. Schwartz, Leonard W.: Comment on "An Empirical Expression for Drag Coefficients of Cones at Supersonic Speeds." AIAA J., vol. 7, no. 3, March 1969, pp. 572-573.

28. Rossow, Vernon J.: Applicability of the Hypersonic Similarity Rule to Pressure Distributions Which Include the Effects of Rotation for Bodies of Revolution at Zero Angle of Attack. NACA TN 2399, 1951.

29. Ehret, Dorris M.; Rossow, Vernon J.; and Stevens, Victor I.: An Analysis of the Applicability of the Hypersonic Similarity Law to the Study of Flow About Bodies of Revolution at Zero Angle of Attack. NACA TN 2250, 1950.

30. Jorgensen, Leland H.: Correlation by the Hypersonic Similarity Rule of Pressure Distributions and Wave Drags for Minimum-Drag Nose Shapes at Zero Angle of Attack. NACA RM A53F12, 1953.

31. Ames Research Staff: Equations, Tables, and Charts for Compressible Flow. NACA Rep. 1135, 1953.

32. Jorgensen, Leland H.; and Redmond, Robert J.: Charts for Equilibrium Flow Properties of Carbon Dioxide in Hypervelocity Nozzles. NASA SP-3015, 1965.

33. Feldman, Saul: Hypersonic Gas Dynamic Charts for Equilibrium Air. AVCO Res. Lab. Research Rept. 40, Jan. 1957.

34. Stivers, Louis S., Jr.: Calculated Pressure Distributions and Components of Total-Drag Coefficients for 18 Constant-Volume, Slender Bodies of Revolution at Zero Incidence for Mach Numbers From 2.0 to 12.0, With Experimental Aerodynamic Characteristics for Three of the Bodies. NASA TN D-6536, 1971.

35. Shapiro, Ascher H.: The Dynamics and Thermodynamics of Compressible Fluid Flow. Vol. II, chs. 26 and 27, The Ronald Press Co., New York, 1953.

36. Sommer, Simon C.; and Short, Barbara J.: Free-Flight Measurements of Turbulent Boundary-Layer Skin Friction in the Presence of Severe Aerodynamic Heating at Mach Numbers From 2.8 to 7.0. NACA TN 3391, 1955.

37. Van Driest, E. R.: Problem of Aerodynamic Heating. Aeronautical Engineering Review, vol. 15, no. 10, Oct. 1956, pp. 26-41.

38. Spalding, D. B.; and Chi, S. W.: The Drag of a Compressible Turbulent Boundary Layer on a Smooth Flat Plate With and Without Heat Transfer. J. Fluid Mech., vol. 18, pt. 1, Jan. 1964, pp. 117-143.

39. Neal, Luther, Jr.; and Bertram, Mitchel H.: Turbulent-Skin-Friction and Heat-Transfer Charts Adapted from the Spalding and Chi Method. NASA TN D-3969, 1967.

40. Hopkins, Edward J.; and Inouye, Mamoru: An Evaluation of Theories for Predicting Turbulent Skin Friction and Heat Transfer on Flat Plates at Supersonic and Hypersonic Mach Numbers. AIAA J., vol. 9, no. 6, June 1971, pp. 993-1003.

41. Hopkins, Edward J.: Charts for Turbulent Skin Friction From the Van Driest Method (II). NASA TN D-6945, 1972.

42. Gabeaud, A.: Base Pressures at Supersonic Velocities. Jour. Aero. Sci., vol. 17, no. 8, Aug. 1950, pp. 525-526.

43. Love, Eugene S.: Base Pressure at Supersonic Speeds on Two-Dimensional Airfoils and on Bodies of Revolution With and Without Fins Having Turbulent Boundary Layers. NACA TN 3819, 1957.

44. Delany, Noel K.; and Sorensen, Norman E.: Low-Speed Drag of Cylinders of Various Shapes. NACA TN 3038, 1953.

45. Polhamus, Edward C.; Geller, Edward W.; and Grunwald, Kalman J.: Pressure and Force Characteristics of Noncircular Cylinders as Affected by Reynolds Number With a Method Included for Determining the Potential Flow About Arbitrary Shapes. NASA TR R-46, 1959.

46. Lockwood, Vernard E.: Effects of Reynolds Number and Flow Incidence on the Force Characteristics of a Family of Flat-Front Cylinders. NASA TN D-3932, 1967.

47. Van Dyke, Milton D.: The Slender Elliptic Cone as a Model for Nonlinear Supersonic Flow Theory. Jour. Fluid Mech., vol. 1, no. 1, May 1956, pp. 1-15.

48. Sims, Joseph L.: Tables for Supersonic Flow Around Right Circular Cones at Zero Angle of Attack. NASA SP-3004, 1964.